E614 Experimental requirements.

1 Introduction.

We propose to measure with high precision for the *first time* the entire differential (in energy and angle) spectrum of positrons from the decay of polarized muons. The main goal of the experiment is the precise testing of the $(V-A)$ structure of electroweak interactions in the framework of the $SU(2)_L \times U(1)$ model.

The decay positron events when reconstructed will provide, ignoring radiative corrections, the double differential spectrum given by

$$\begin{aligned}\frac{d^2\Gamma}{dx d(\cos\theta)} &= (x^2-x_0^2)^{1/2}\left\{6x(1-x)+\frac{4}{3}\rho(4x^2-3x-x_0^2)+6\eta x_0(1-x)\right. \\ &+ \left. P_\mu\xi\cos\theta(x^2-x_0^2)^{1/2}\left[2(1-x)+\frac{4}{3}\delta(4x-4+(1-x_0^2)^{1/2})\right]\right\} \qquad (1)\end{aligned}$$

$$\text{with} \quad x=\frac{E_e}{W_{\mu e}}, \quad W_{\mu e}=\frac{m_\mu^2+m_e^2}{2m_\mu}, \quad \text{and} \quad x_0\equiv\frac{m_e}{W_{\mu e}} \le x \le 1.$$

P_μ is the muon polarization. θ is the angle between the muon spin direction and the positron momentum, $\cos\theta = \hat{S}_\mu \cdot \hat{p}_e$, and ρ, η, ξ and δ are the Michel[1] parameters, the present knowledge of which is summarized below:

parameter	standard model value	experimental value[2]	present uncertainty ($\times 10^{-4}$)
ρ	3/4	.7518	26
η	0	.007	130
ξ	1	1.0027	84
δ	3/4	0.7486	38

Since E614 will measure the Michel parameters simultaneously a significant reduction in the systematic error will be achieved. $\Gamma(x,\theta)$ will be measured over a range of x and θ in order to determine the four Michel parameters with the significantly improved accuracies;

$$\sigma(\rho) = [\pm 5(stat) \pm 9.2(syst)] \cdot 10^{-5}$$

$$\sigma(P_\mu\xi) = [\pm 10(stat) \pm 10(syst)] \cdot 10^{-5}$$

$$\sigma(\delta) = [\pm 8(stat) \pm 9.5(syst)] \cdot 10^{-5}$$

$$\sigma(\eta) = [\pm 160(stat) \pm 500(syst)] \cdot 10^{-5}$$

The listed statistical error estimates are discussed in section 4 while the systematic error estimates are summarized in Table 9 in section 6 where reference to the section in which they are discussed can be found. Estimates of the systematic uncertainties for η do not appear in Table 9 because they are very preliminary, we hope that it is possible to reduce the estimate given here. Our η result would still be a factor of $\sim$2 better than the present value.

The E614 experiment consists of essentially two segments, the M13 channel which functions as the source of polarized muons and a spectrometer which analyses the positrons from the decay of these polarized muons. Fig. 1 presents schematically the components of this apparatus, including the BL1A proton beam (500 MeV), the BL1A meson production target (1AT1), the M13 meson

channel (viewing the production target at 135 degrees and consisting of 7 quadrupoles, 2 dipoles and a momentum defining slit), the time expansion chamber(TEC) and the spectrometer. The E614 spectrometer itself consists of two components(see Fig. 1), a super-conducting solenoid and an array of planar wire chambers, shown schematically in Fig. 2, installed in the center of the solenoid.

The 100% polarized 4.1 MeV surface muon beam from M13 will be brought to rest in an aluminium foil(stopping target) at the center of the magnetic field. When the stopped muons decay all trajectories of the resulting positrons will be confined to the central $36cm$ diameter volume where they will produce hits in a set of planar chambers mounted symmetrically upstream and downstream of this foil. The result will be, for the first time, a measurement of the entire Michel spectrum.

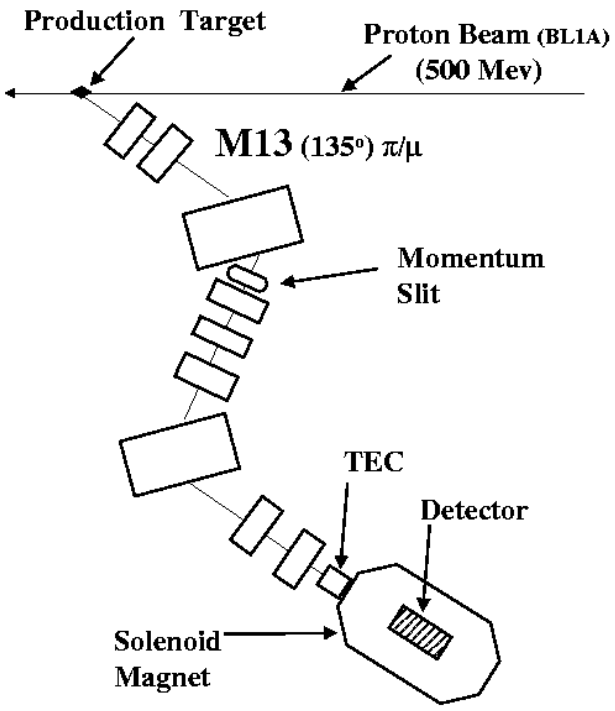

Figure 1: Schematic of E614 experiment from the meson production target (1AT1) to the spectrometer.

Fig. 2 shows schematically the upstream half of the complete detector array to be inserted into the spectrometer magnet.

The following list explains the structure of the upstream detector assembly beginning at the upstream end. The downstream section is an exact mirror image, even containing a scintillation trigger counter for reasons of symmetry. Referring to Fig. 1 and Fig. 2:

- The time expansion chamber(TEC) measures the muon momentum vector, hence P_μ, before the muon enters the fringe field region of the spectrometer.
- The scintillation counter measures the deposited energy of beam particles in order to distinguish incoming positrons, muons or pions and provides the trigger signal.

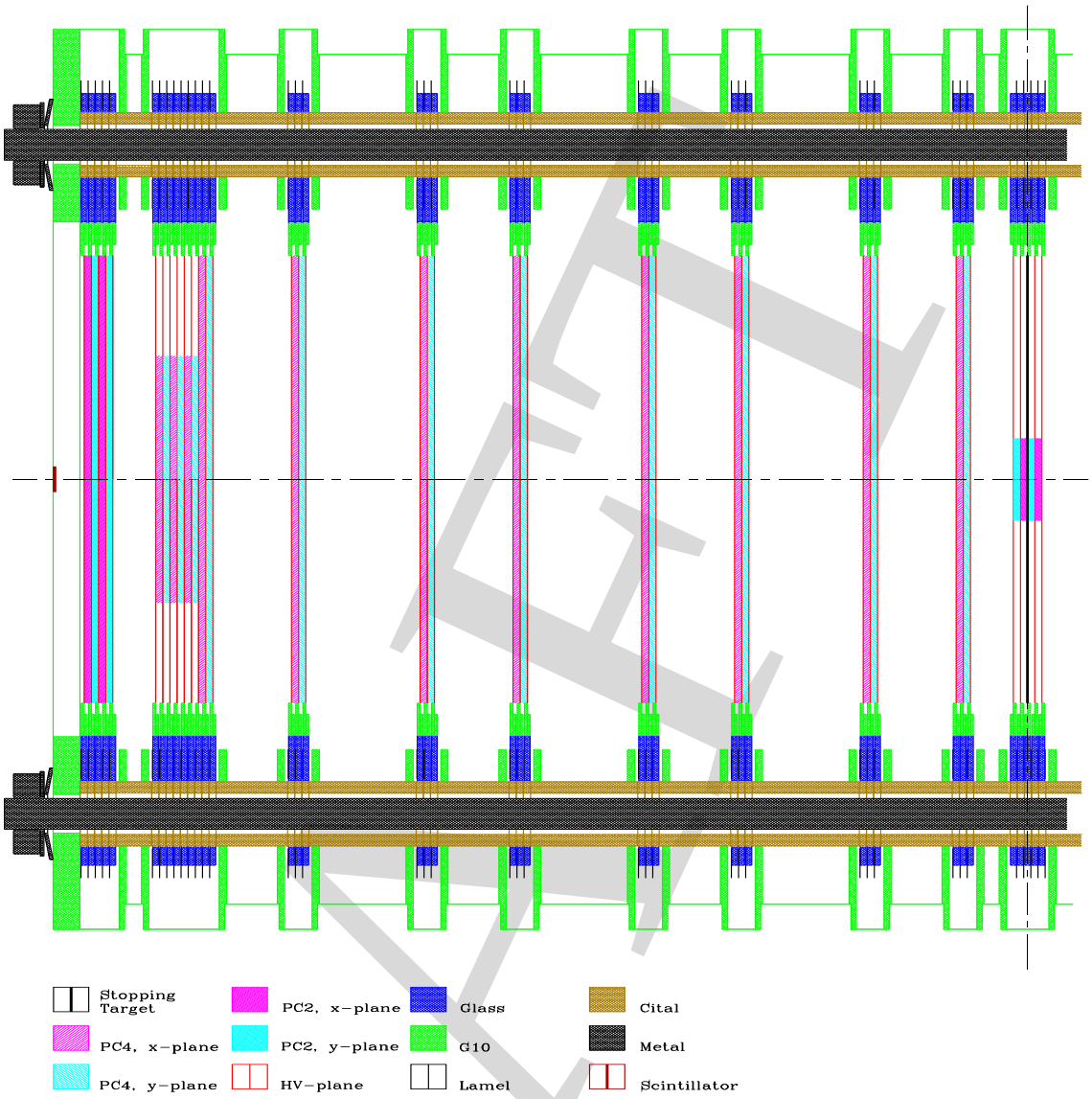

Figure 2: Schematic layout of half the E614 detector assembly. Here PC2 and PC4 identify the PC and PDC planes respectively.

- A set of proportional chamber (PC) planes serve to measure the muon beam spot size and its mean position with a spatial resolution of $\sigma = 0.6mm$.
- The tight set of planar drift chamber (PDC) planes serve as an additional tool to distinguish between small radius helices with short and long periods (low positron energies or small angle θ).
- Eight pairs of (X+Y) PDC planes serve as the primary detector of the positron helices. They are separated by $40mm$ and $60mm$ gaps filled with helium gas. The latter have been introduced to improve the track reconstruction accuracy for small polar angles (θ) of outgoing positrons.
- The $20mm$ helium gap between the last PDC pair and the PC pair before the stopping target is needed in order to separate an incoming muon from outgoing upstream positron when the positron is emitted at a small angle.

- The PC before the stopping target and the identical PC after the target are used as indicators of muon stops inside the target. These PCs can also provide a first guess for time zero, t_0, for the conversion of the drift chamber times to distances.

The PC's at the target and the PDC's in the dense stack will contain a full complement of wires but only those in the shaded regions of these chambers will be read out for reasons of economy. These regions represent 32 wires in the PC's and 48 wires in the PDC's. Further details on this detector array, the construction materials and procedures, the demands imposed on the detector by the experiment and the solutions to these demands are presented below in subsection 3.2.

The surface muon source and the delivery system, M13, are discussed below in section 2. The spectrometer, including the detector array is presented below in section 3. In these two sections, 2 and 3 the demands imposed by the desired results and how they will be resolved are described. The experimental tests and the Monte Carlo studies that verify these solutions will also be presented in these two sections. Section 6 presents, in tabular form, a summary of the systematic corrections and uncertainty estimates. Section 5 is a presentation of the schedule for installation and operation of the experiment. The last section summarizes this report.

2 μ beam requirements.

The fact that our results will depend on how close the polarization of the muons, P_μ, is to 100% and how accurately this polarization is aligned with the magnetic field (P_μ^z) at the point in the stopping target where they decay puts very strict requirements on the delivery of the muon beam to that point. Any mechanism that reduces P_μ^z must be minimized. This means that the entire μ delivery system, from the production target (1AT1) to the stopping target must be considered as part of the experimental apparatus. In what follows any mechanism that alters the relationship between the muons momentum and the direction of its spin axis is referred to as a cause of *real* depolarization of the muon while any effect that reduces the alignment of the stopped μ's spin with the axis of the spectrometer magnetic field is referred to as a cause of *apparent* muon depolarization.

In the Standard Model the $\pi^+ \rightarrow \mu^+\nu$ decay at rest results in P_μ of 100%. The M13 surface muon beam is produced when pions stopped in the surface of the production target decay, this beam is therefore expected to be 100% polarized. The challenge is to preserve this polarization and deliver it, aligned to the axis of the magnet, to the stopping target, the ideal being P_μ^z equal to P_μ or 100% if the Standard Model correctly describes π decay. There are several factors which can degrade P_μ^z. Multiple scattering, for example, changes the momentum direction of the muon but does not affect the muon spin direction, thus it reduces the real polarization, P_μ. The fringe field of the spectrometer magnet can impart transverse momentum to the muon resulting in a misalignment of P_μ with the magnetic field axis, i.e. a reduction in P_μ^z (an example of an apparent reduction in P_μ). Similarly the consequence of a misalignment between the muon beam axis and the spectrometer magnetic field will be a reduced P_μ^z. Muonium(μ^+e^-) formation in the materials of the spectrometer can result in a real reduction of P_μ since this allows for spin exchange between the randomly oriented electron and the muon. This begins to occur when the muon energy has been reduced to $\leq$ 100 keV, i.e. in the neighborhood of the stopping target.

2.1 Production target influences.

The magnification of the M13 channel is 0.84 at the momentum slit and $\approx$ -1.5 at the final (experimental) focus. This means that motion of the proton beam on the production target will influence momentum selection and the position of the muon beam at the point where it crosses the fringe field of the spectrometer magnet. (As will be explained later it is intended to have the M13 final focus at

this latter point.) For example, a $5mm$ movement of the muon source will translate into a change at the center of the momentum slit of $\approx 0.35\%$ in momentum and to a movement of the final focus by $\approx 7.5mm$. A change in the selected momentum will mean a change in the selected muon polarization (see the discussion of multiple scattering in the production target below). Movement of the beam at the spectrometer entrance will mean a change in the amount of transverse momentum imparted to the muons due to the spectrometer fringe field. The average apparent muon polarization at the point of decay in the stopping target will be different as a result. Changes as large as these, $\Delta p = 0.35\%$ and $7.5mm$ will produce unacceptable effects and are therefore not acceptable.

Several solutions are available to achieve proton beam stability at $\leq 1.0mm$. The present instrumentation in BL1A is sensitive to $0.5mm$ shifts in the position of the proton beam so that maintaining stability to $\sim 1mm$ is possible. The simplest is to use this device to monitor the beam position and return it to a "standard" position if it wanders. The counter(TEC) at the front end of the spectrometer can also be used for this purpose but it also sees beam movement due to instabilities in the muon beam transport system(see section 2.2). The present parity experiment at TRIUMF employs a feedback system that allows them to maintain the proton beam centroid to $\sim 1\mu m$ accuracy over hour long runs. Such a system will be studied for use in BL1A. If none of these approaches proves to be adequate the production target will be slanted in such a way as to make the proton beam spot invisible to M13 so that any motion would not affect the muon beam position at either focus. Small movements of the proton beam, $\leq 1mm$ produce momentum selection changes of less than 0.07%, a negligible influence on the selected muon polarization. A movement of $\sim 2mm$ at the spectrometer entrance is equivalent to an angle between the muon beam and the magnet axis of $2mm/1500mm$ radians, a negligible apparent P_μ^z reduction of $\sim 10^{-6}$. This $2mm$ transverse displacement of the muon beam in the fringe field area at the entrance to the solenoid could also cause additional changes in $(1 - P_\mu \xi)$ of order $\sim 5 \cdot 10^{-5}$ through increased transverse momentum imparted to the muon. This is the figure which is conservatively quoted in Table 9. However, the measurement of the muon trajectories with the TEC is expected to reduce all such influences to a negligible level.

A GEANT-based Monte Carlo study of surface muon production was undertaken to determine the influence of target geometry on the surface muon beam areal distribution and to determine the influence of depth below the target surface at which the muon was produced has on the muon polarization, P_μ. In the first of these Monte Carlo studies the proton beam had a normal distribution density in the transverse plane with standard deviations σ_x and σ_y in the horizontal and vertical directions respectively. For the purposes of the study σ_x and σ_y were taken from those presently employed in actual beams. We have updated the physics routine employed by GEANT to calculate pion production probabilities (Gheisha), replacing the extrapolation from high energies with one from cross sections measured near the 500 MeV available at TRIUMF. The resulting pion energy and angular distributions are very significantly different from those of the original Gheisha. The GEANT routine follows the produced pions until they stop and decay, or escape the target. In the latter case they are subsequently ignored but in the former case the decay muons are tracked. If a muon escapes the target, its exit position and its momentum are recorded. This muon distribution is used as the input to REVMOC studies, presently underway, of the M13 channel.

In the second part of the 1AT1 Monte Carlo studies, pions were generated at rest at a fixed distance below the 1AT1 (assumed to be made of graphite) surface. GEANT immediately decayed these pions generating 29.79 MeV/c muons whose directions in space were random. Each muon was then tracked to the target surface and the difference between its original momentum and that at the surface was calculated. Since the multiple scattering which produces this difference does not influence the direction of the muons spin, this difference is a measure of the muon "depolarization". Figure 3 shows this depolarization as a function of depth within the target of the original pion decay position. In this study the muon was accepted if, when it left the surface, its direction was within a cone of either θ_{max}=10^o or θ_{max}=1^o. For reasons of computing time, the 10^o limit was used

for most of the calculations appearing in this figure. No significant difference was found between these cases (the average path length to the surface is less than 2% longer for the larger angle). The momentum of the selected muons and their "polarization" was of course degraded in direct proportion to the depth from which they originated. The desire to be able to select muons of the highest "polarization", i.e. those from as close to the production target surface as possible indirectly puts a restriction on the 1AT1 target size. The momentum selection slits in M13 are positioned at a focus where the momentum dispersion is $\approx 1.22cm/\%\Delta p/p$. This means that with the present 1AT1 target the minimum momentum bite will be $\approx$1%. To further examine this problem two runs were made in which the original pion was randomly generated up to $100\mu m$ below the target surface. These runs, with "perfect" momentum selection, requiring that the accepted muons have momenta of greater than 29.5 and 29.25 MeV/c (1% and 2% acceptance respectively), resulted in the two filled squares in Fig. 3. Since the real momentum selection will be related to the production target size an optimization would suggest that a smaller($\leq 7mm$) 1AT1 is required to allow selection of those muons that are less depolarized. From Fig. 3 it is seen that $(1 - P_\mu) \sim 5 \cdot 10^{-5}$ is available with Δp/p = 1% momentum selection. This effect will be studied experimentally by reducing the muon beam momentum, hence sampling muons produced deeper in the target. It is estimated that these measurements will allow determination of the shift in $(1 - P_\mu \xi)$ to better than $\pm 1 \times 10^{-5}$.

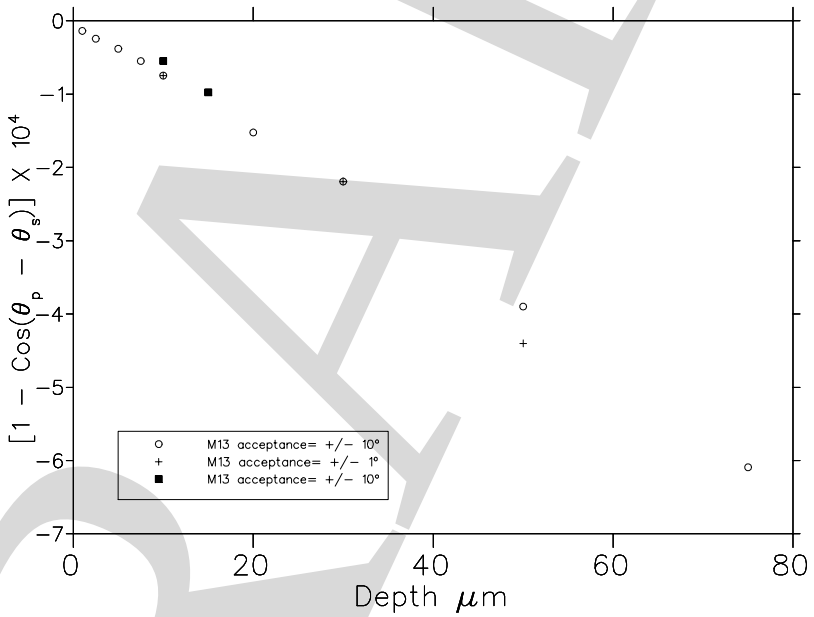

Figure 3: Muon "depolarization" in the 1AT1 Target. Here θ_p and θ_s are the final and initial momentum directions respectively.

2.2 μ beam transport system influences.

A minor effect that causes real muon depolarization is the scattering of μ's that encounter the edge of a slit while traveling along the beamline. Studies indicate that slit edge scattering has a rather small effect on the polarization distribution for the selected muons. This result may be understood when one considers that since the muons with degraded polarization have also lost momentum many will not be transported through the channel. Monte Carlo (REVMOC) calculations with slits of thickness $5cm$ have been found to decrease the average muon polarization by only 1.44×10^{-4}. Nonetheless, we plan to replace the slits in M13 to minimize this effect. It is estimated that by using slits with

edges which are $0.1mm$ thick, the resultant depolarization can be kept to a few parts in 100,000. These studies will continue and will be compared to tests to be made in M13.

Two major contributors to apparent depolarization of the μ's are impurities in the muon beam and any transverse momentum imparted to the muons as they cross the fringe field of the spectrometer solenoid. Impurities such as pions and cloud muons masquerading as surface muons would obviously reduce the apparent average polarization of the "surface" muon beam and through their decay may be a source of positrons that, if mistakenly identified as originating from the decay of a polarized surface muon would distort the Michel spectrum. Decreasing the contamination in the beam is therefore a necessity and this places requirements on the stability of the M13 magnets. Transverse momentum changes, due to movement of the μ^+ beam, and their relationship to apparent polarization were discussed above in the section on the stability of the proton beam position, here we are concerned with motion of the beam due to M13 magnet instability. Minimization of both these depolarization mechanisms will be significantly improved by achieving higher stability of the magnets in the M13 channel through upgrades to the control and monitoring of same.

The non surface muon components of the M13 beam at p_0=29.6MeV/c, given in Table 1 were determined in a test run in 1995.

Table 1: M13 surface μ beam impurities per surface muon(PSM).

Contaminant Particle	Measured rate /surface muon	Rate after corrective action
e^+	4	$\leq 2 \times 10^{-5}$
π	2.9×10^{-3}	$\leq 3 \times 10^{-7}$
μ(cloud) from 1AT1	2.1×10^{-2}	$\leq 6.7 \times 10^{-6}$
μ(cloud) from S0	3.4×10^{-4}	$\leq 1.1 \times 10^{-8}$
μ(non-surface) in "usable" time window	6.7×10^{-5}	$\leq 6.7 \times 10^{-6}$

The large time window, 44 nsec, between proton beam pulses at TRIUMF provides the best mechanism for reduction of these contaminants. The time of flight of particles from the production target through M13 is measured between the capacitive probe in beam line 1A and the scintillator at the front end of the spectrometer. It is possible to select a time window, $\geq 16ns$ long, in this TOF spectrum in which there are essentially no contaminant particles. Reduction of the non-surface muons that appear in this "usable" time window requires that further measures be taken. The action required includes replacing the material in the channel slits with thinner pieces, changing the production target to the short version and improving the control and monitoring of the M13 magnets. The latter will assure stability of the TOF cut discussed here. Pulse height analysis of the signal from the scintillator at the spectrometer entrance will also provide a very significant rejection factor for the positrons in the beam. The expected levels of each contaminant remaining per surface muon after all cuts and corrective measures have been taken are listed in Table 1. The time structure of the TRIUMF beam thus means that TRIUMF provides the best source of highly polarized surface muons available for E614. The most pessimistic assumption is that a long tail exists on the cloud muon peak, this would then be the main source of any non-surface muon admixture. If this is the case the estimate for the existing target (given in Table 9) would be $(1 - P_\mu \xi) = (12 \pm 3) \cdot 10^{-5}$.

A source of contaminant particles that cannot be removed with the TOF cut are the positrons from surface muon decay in flight. The influence of these positrons on the Michel spectrum has been estimated to be negligilble since they will only be included in the spectrum if the decay occurs in the stopping target. The probability of a muon in motion decaying in the target is very small,

$\sim 10^{-6}$. This possibility will be reduced even further by the delay we will impose on the opening of the positron "gate".

As mentioned above, improvements in the stability of the muon beam reduces motion of the beam where it crosses the fringing field of the solenoid thus reducing any changes in the apparent depolarization that occurs at this point. An estimate indicates that a current change of order 10^{-3} in the M13 dipoles would cause a shift of $1 - P_\mu \xi < 10^{-5}$. The M13 magnet power supply monitoring will be improved to assure better than 10^{-3} accuracy and NMR and Hall probes will be installed in the magnets. Taking a conservative view, the number that is entered into Table 9 reflects the result above. Two other measures will also be taken to help reduce this effect to a minimum. The jaws at the front end of M13 will be set to optimize the beam rate while minimizing the surface muon beam emittance. A small emittance beam is easier to transport into the solenoid and besides the angular divergence of the beam is directly related to P_μ^z. The measured flux for a $126mm - mrad$ M13 surface muon beam with a 150μA proton beam at 1AT1 was 5.75k. The second measure that will be taken to reduce the transverse momentum impulse in the fringe field is the installation of a specially designed entry port to shape this field where the beam enters the solenoid. In addition, the measurement of the incoming muon trajectory with the TEC and with the PC's at the entrance to the detector will mitigate, if not eliminate the influence of beam motion at this point. It is estimated that these effects will therefore have negligible influence on $(1 - P_\mu \xi)$.

As mentioned in section 2.1 a new shorter production target will improve the M13 momentum selectivity and consequently discrimination of the depth within the production target from which the muon originated. Improved M13 magnet stability, in combination with this new target, will allow for maintaining the level of depolarization at the selected level.

2.3 Influences of spectrometer materials on P_μ^z.

μ depolarization in detector materials will occur through the formation of muonium with subsequent spin exchange occurring between the electron and muon. This does not occur in general in pure metals where the lifetime of any muonium that is formed is too short to allow the spin exchange to happen. All possible mechanisms of muon depolarization in the Al stopping target have been analyzed with the conclusion that all lead to depolarizations that are very small at $B = 2T$ if the admixture of ferromagnetic elements (Fe,Co,Ni) in Al is less than $10ppm$. Obviously the target material will be the highest grade Al possible.

On the other hand muonium can form in many of the materials that make up the detector and may last sufficiently long enough for this spin exchange process to occur. It is necessary to prevent muons stopping in such materials or to be able to "cut" such events during the analysis stage. This issue will be addressed by the use of the proportional chambers adjacent to the stopping target. Nominally the trigger condition $\mathrm{PC}(-2) \cdot \mathrm{PC}(-1) \cdot \overline{\mathrm{PC}(+1) \cdot \mathrm{PC}(+2)}$ removes such events. The notation adopted here is that PC(-2), PC(-1) refer to the upstream proportional chambers while PC(+1), PC(+2) refer to the downstream chambers.

However, this simple scheme may not account for those muons that could lose all their energy and stop in PC(-1), nor does it account for those muons that nearly stop in the target and lose a small amount of energy in PC(+1). The addition of ADC's to the PC's will solve this problem by allowing for a measurement of the energy loss. Monte Carlo simulations were performed to determine if with this extra information, one could impose cuts that eliminate those muons stopping in PC(-1). In the simulation a beam of 29.7 MeV/c μ^+'s were tracked until they stopped and were allowed to decay, the resulting positrons were not tracked. As muons entered and exited the PC's, their kinetic energy was recorded and their energy loss in each chamber was histogrammed.

The mean energy loss per muon in the chambers was $\sim$0.1 MeV. The distributions of energy loss in PC(-2), PC(-1) ,PC(+1), and PC(+2) are shown in Fig. 4. A scatterplot of energy losses in

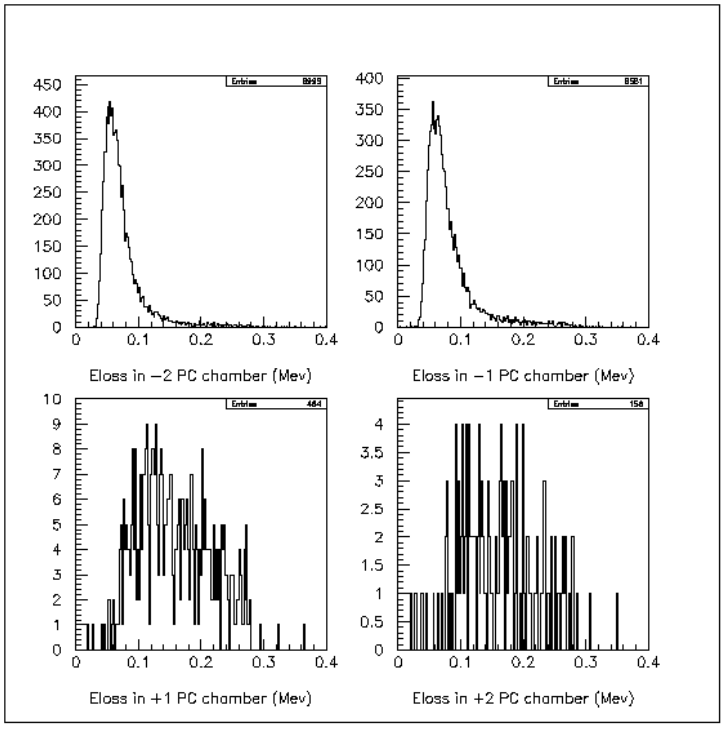

Figure 4: Muon kinetic energy loss in PC(-2),PC(-1),PC(+1), and PC(+2) chambers for an initial 10,000 events.

x-intercept of the cut line (MeV)	% stopping in PC(-1)	% stopping in target
0.151	7.3	98.7
0.144	2.3	98.2
0.137	0.6	97.3

Table 2: μ^+ stopping percentage in the target and PC(-1) as a function of x-intercept of 2-D cut.

PC(-2) and PC(-1) is shown in the upper-left of Fig. 5 and exhibits two main features: a dense locus of points with a positive slope and a less dense locus with a negative slope. The dense locus with positive slope is due to muons stopping in the target (Fig. 5, bottom left), and the low energy end of this locus is due to those that pass through the target(Fig. 5, bottom right). The less dense locus of negative slope is due to muons stopping in PC(-1).

As seen in Fig. 5, nearly all stops in PC(-1) have an energy loss in PC(-2) greater than ∼0.1 MeV, so a cut at that value would remove most events with stops in PC(-1). A two dimensional cut along the lower edge of the locus of PC(-1) stops would be more efficient. The equation of the cut line is approximately $\Delta E(-2) = -1.74 \times \Delta E(-1) + a$ MeV. Table 2 shows the results for various values of the x-intercept, a, that attempt to minimize stops in PC(-1), while maximizing those that stop in the target. Of the 3.5% of the incident muons that stop in PC(-1) only 0.6% remain after the cut with x-intercept = 0.137 MeV has been implemented. This means that the stops in PC(-1) will be reduced to $2 \cdot 10^{-4}$ of the incident flux while more than 97% of the muons stopping in the target will be kept.

It is expected that the energy threshold of the PC's will be at most ∼1 keV. From Fig. 4 it is seen that the smallest energy loss recorded by PC(+1) is ∼20 keV. In 10,000 entries, there were no muons that lost less than 1 keV of kinetic energy. Providing the chamber thresholds can be kept low

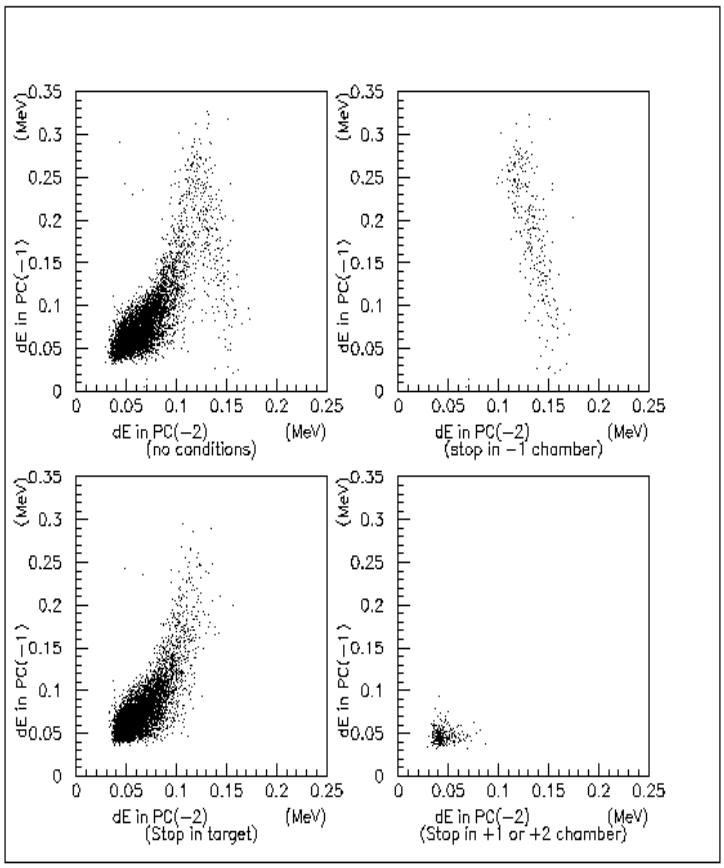

Figure 5: Energy loss in PC(-2) and PC(-1) chambers for various muon stopping conditions. Top left: no conditions; top right: stop in PC(-1); bottom left: stop in target; bottom right: stop in PC(+1) or PC(+2).

($\leq$ 5 keV), it is therefore unlikely that muons will pass through the target and not be recorded by PC(+1). Pessimistically assuming that the PC(+1) energy threshold is 25 keV, ~ 2 stops in PC(+1) will be missed by a cut at this level per 10^4 stops in the target.

The measured P_μ value for muons stopped in $CF_4(ISO)(80:20)$ gas at $B = 2T$ is $P_\mu > 0.985$. According to the above Monte Carlo calculations $\leq 2 \cdot 10^{-4}$ muons stop in PC(-1) and in PC(+1). The shift of $(1 - P_\mu \xi)$ is therefore pessimistically estimated to be $(1 - 0.985) \times 5 \cdot 10^{-4} = 7.5 \cdot 10^{-6}$.

Muon depolarization is possible in solid films which may form on detector wires or on the surface of stopping target. In [3] the thickness of the solid film formed on the surface of a PC anode wire was measured after an accumulated charge $\approx 5C/cm$ which corresponds to more than 10^{12} detected particles per cm of sense wire. The mixture CF_4/ISO (80/20) was used as the drift gas. The measured thickness of the film was ~ 20 Å. In our experiment we are going to detect no more than 10^9 particles per sense wire, a long way from $10^{12}/cm$. The number of muons which will stop in the resulting film, much thinner than 20 Å, will be very small and we shall therfore neglect the influence of such a film on muon depolarization. Note also, that many publications state that a CF_4/ISO gas mixture does not interact chemically with aluminum. The drift gas may also permeate into pores and structure disturbances of the aluminum foil target which could then lead to muon depolarization in such places. This effect is also considered to be negligible.

2.4 Optimizing P_μ^z and the μ stopping distribution.

Two factors are involved in optimizing the mean polarization, P_μ^z and the μ stopping distribution. The muon beam that emanates from the M13 channel has a focus which can be positioned along the Z-axis relative to the spectrometer by tuning the magnetic quadrupoles at the end of the beamline, or by positioning the spectrometer appropriately. Several Monte Carlo studies have been made of the optimization of the position of this focus versus the flux of highly polarized muons stopping in the target. The second factor that has been examined with Monte Carlo is the distribution in z within of the stopping target of these muons, symmetry in z being the ideal. Details on the studies summarized in this subsection can be found in E614 Technotes 7, 14 and 22.

2.4.1 M13 focus position

The optimum position for the muon beam focus is suspected to be near the region, known as the "fringe field," where the magnetic field increases from zero in the beamline to a uniform 2.2 T inside the spectrometer. This is approximately where the radial component B_r of the magnetic field is a maximum. The first goal of the Monte Carlo studies (performed using GEANT) was to find this optimum. The second goal was to find a "tuning" technique that would make it possible to experimentally optimize the focus location.

A beam of surface muons generated by REVMOC using a standard M13 tune were employed as input for a study of the positioning of the focus. This study employed a spectrometer magnetic field generated by Opera2d for the "standard" E614 magnet plus shield package. The focus position, L, of each muon track was plotted versus the spin if that muon stopped in the target. Fig. 6 reveals that the stopped muons with the highest aligned spin tend to have foci near $z = -150cm$. Selecting only those muons for which $P_\mu^z < -.9995$, the mean value of L is $-141.3cm$, with a standard deviation of $\sigma_{\overline{L}} = 77.6cm$.

2.4.2 Optimizing P_μ^z.

A central goal of the E614 experiment is to measure the product $P_\mu \xi$ to a precision of less than three parts in 10^4. The mean depolarization, $(< 1 - P_\mu^z >)$ must therefore also be less than three parts in 10^4. Several techniques for selecting, from the incoming muon beam, an ensemble of muons that stop in the Al foil target that also satisfy this polarization requirement have been examined.

The simplest way for selecting particles in a beam is to place a physical slit in the path of that beam. Since Fig. 6 indicates that it should be possible to make the muon polarization selection based on position at the focus, a slit was simulated at that location. The polarization selectivity was found to be insufficient. Since the spin of the surface muon is opposite its momentum vector and high polarization refers to muons with spins with large z components in their spins, it follows that a high P_μ^z ensemble of muons will be those that travel in helices with small radii. Consideration was therefore given to the possibility of either using the PDC's of the positron detector or a special set of "muon detector" PDC's for determining the muon helix. Fig. 7 compares, as a function of focal position, the true mean polarization of the stopped muons and their mean polarization as predicted from the fitted helix, in this case as determined by the positron detector PDC's. The result with the "muon detector" was only marginally better. This technique does not provide the required selectivity. Another approach, that used in a previous experiment[4][5], is to measure the muon trajectory before the muon encounters the fringe field (i.e. where the trajectory is linear). To determine if such a measurement would provide the desired information on the stopped muon polarization two simulated PDC's were placed in the beamline, upstream of the fringe field. The multiple scattering in these detectors modified the relationship between the muon momentum and

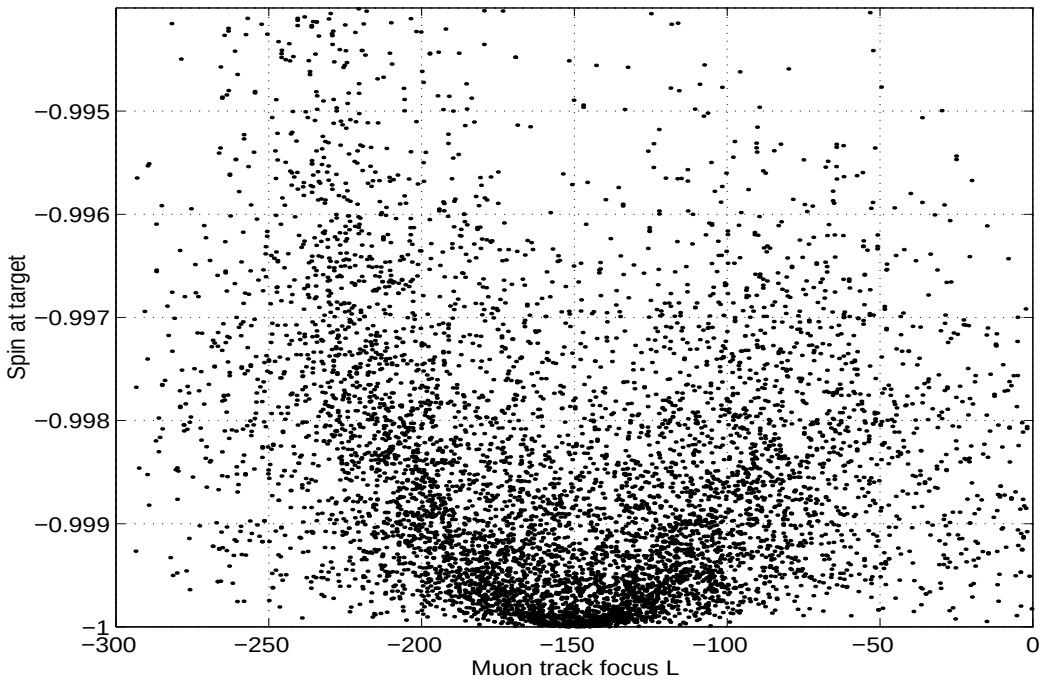

Figure 6: Spin at target vs. muon track focus L. ($L = -300 + r_i \frac{P_z}{P_r}$). The distribution of data points seems to indicate that the optimum focus position for the M13 beam would be at $z = -150cm$.

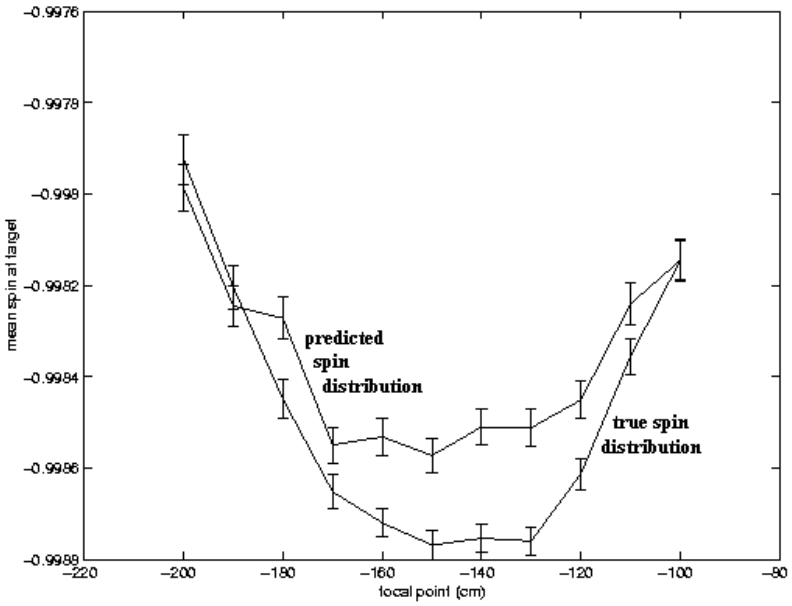

Figure 7: The impact of the focal point on the mean z component of the muon spin(polarization) at the target.

the muon spin so much that the results could not be used to make a selection. It was therefore decided to study the employment of a very low mass device, such as a Time Expansion Chamber

(TEC), in this position. In Monte Carlo simulations, such a chamber was placed upstream of the solenoidal fringe field. The TEC simulated is shown in Figs. 8 and 9. This chamber is designed to be operated at 20 Torr and will have only two very thin ($6\mu m$ & $100\mu m$) windows in order to minimize energy loss and multiple scattering effects on the incoming muons. The $6\mu m$ window will separate the low pressure chamber gas from the M13 beamline vacuum and the $100\mu m$ window will separate the former from the atmospheric pressure He gas inside the spectrometer volume. The chamber will be positioned (see Fig. 9) so that the xz and yz measuring sections are just before the entry port in the spectrometer steel, which is $\sim 160cm$ upstream of the stopping target. The choice of DME as the drift gas was made because of the small Lorentz angle that will result due to the fringe field in the region of these detectors. In the highest field in this region the Lorentz angle will only lengthen the electron path by $\sim 30\mu m$. The estimated number of electrons in the DME created by the passage of a surface muon is $2.6/mm$ and the drift velocity will be $15\mu m/nsec$ at E/p=5V/cm-Torr. The estimated errors on the track position and angle are $\pm 50\mu m$ and $\pm 2mrad$ respectively. Further details on the design considerations are contained in E614 Technote 17.

In the simulation of the TEC the output of the chamber was used to reconstruct the incoming muon track. Correlations between the reconstructed angle with the spin direction of the muon as it stopped in the target were studied. A cut on the polar angle of the initial muon track as measured by the TEC was found which retained ~12% of all muons stopping in the target(~78% of the M13 flux) while reducing the mean depolarization $< 1 - P_\mu^z >$ of the retained events to $\sim 2 \times 10^{-4}$. This result was obtained using a highly convergent beam with a focus at the fringe field region, $160cm$ upstream of the target. This tune is representative of a standard M13 beam that would normally be focussed in such a manner, but usually at the exerimental target. A more parallel beam was found to produce poorer results. The spatial resolution of the TEC, assumed to be between 50 and 200 μm, had only a small effect on the results. This success of the TEC concept has led to the decision to complete the design work with the aim of testing a prototype next summer. Monte Carlo studies to search for an M13 tune that optimizes the percentage of muons with mean depolarization $< 1 - P_\mu^z > \leq 2 \times 10^{-4}$ will be carried out. In the meantime this number is entered into Table 9 as the μ Track Projection correction/uncertainty.

2.4.3 Optimization of the μ stopping distribution.

A scatterplot of the muon energy losses in PC(-1) and PC(-2) was considered as a monitor of the stopping distribution in the target. In Fig. 10 three stopping distributions along with their corresponding energy loss scatterplots are displayed. A symmetric stopping distribution (Fig. 10, middle) is produced by placing a 340 μm thick scintillator in the muon path. By decreasing the thickness to 320 μm a stopping distribution skewed toward positive z is produced (Fig. 10, top). A skew to negative z is achieved by increasing the thickness to 360 μm (Fig. 10, bottom). These scatterplots are very similar and, except for a slight energy displacement, do not show any qualitative difference. The energy displacements suggest mean energy loss as a monitor of stopping distribution. However, this would require precise calibration of the detectors, since differing thresholds, gains, and efficiencies could cause artificial shifts in the mean energy loss.

A simpler method is merely to count the number of muons passing through the proportional chambers. The ratio of the number of muons recorded by PC(+2) to those recorded by PC(-2), and the ratio of PC(+1) to PC(-1) should change with deviations from a symmetric stopping distribution. These ratios should not be affected by factors such as PC efficiency (unless each chamber has different efficiency) or muons stopping in PC(-1). Other ratios change as well, but $N_{PC(+1)}/N_{PC(-1)}$, and $N_{PC(+2)}/N_{PC(-2)}$ were found to be the most sensitive to changes in the stopping distribution.

For a symmetric stopping distribution, Table 3 shows that the ratios, $N_{PC(+1)}/N_{PC(-1)}$, and $N_{PC(+2)}/N_{PC(-2)}$ were 0.054 and 0.0173, respectively. Deviations of $\pm 20\mu m$ in scintillator thickness

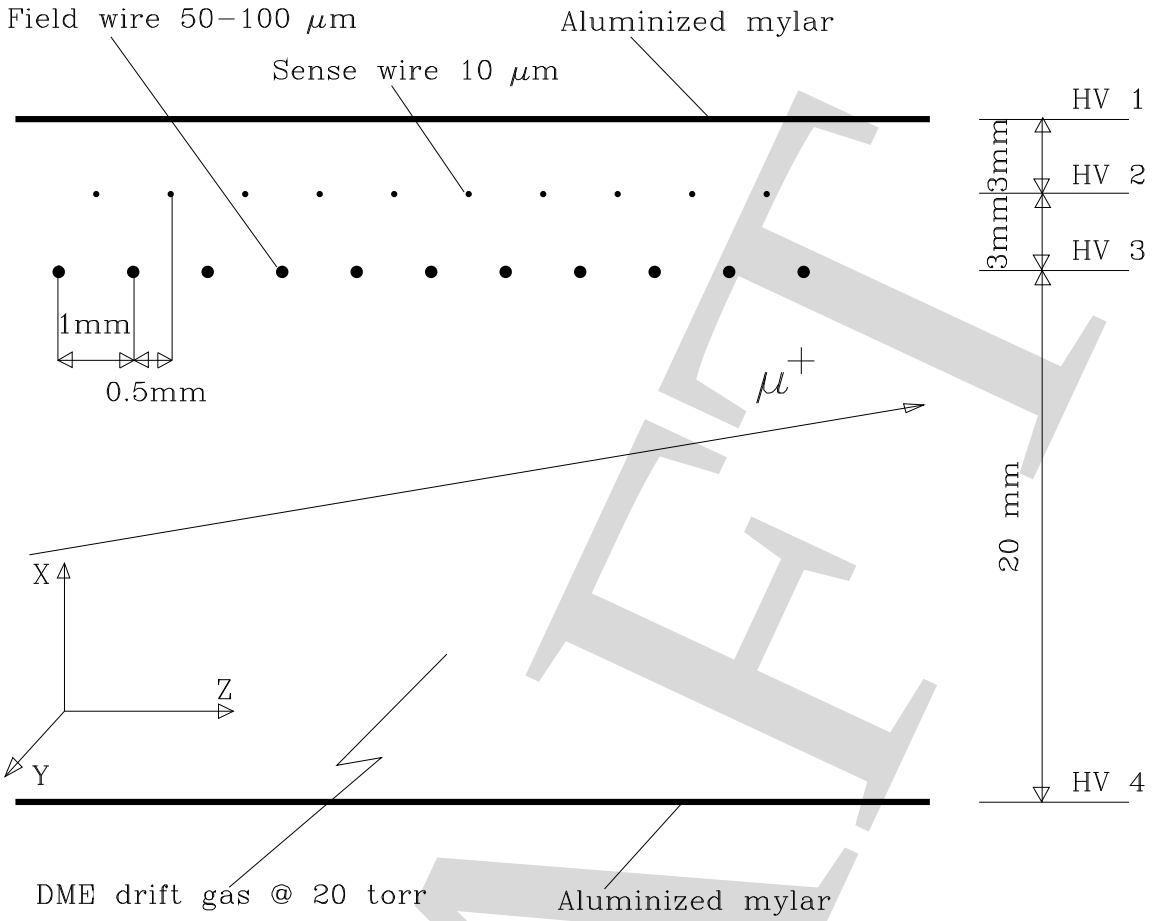

Figure 8: Sketch of time expansion chamber(TEC). Drift region is between HV3 and HV4 planes. Amplification region is between HV3 and HV2.

produced a significant change in ratios. These ratios are statistically robust. For example, the ratio $N_{PC(+2)}/N_{PC(-2)}$ for the right-skewed distribution is 16σ different from the same ratio in the symmetric case. These ratios are therefore very sensitive to differences in the stopping distribution, and are shown graphically in Fig. 11.

The central PC's provide a reliable monitor of stopping distribution when the ratios of the number of muons recorded by PC(+2) and PC(-2) and PC(+1) and PC(-1) are examined.

stopping distribution	mean in z (μm)	number in PC chamber				Ratios	
		-2	-1	+1	+2	+2/-2	+1/-1
symmetric	0.18	8999	8581	464	156	0.0173 ±0.001	0.054±0.003
right skew	4.9	9327	9021	986	443	0.0475 ±0.002	0.109±0.004
left skew	-5.6	8533	7910	176	39	0.0046 ±0.001	0.022±0.002

Table 3: Ratios of number of muons recorded by the proportional chambers as a function of stopping distribution mean.

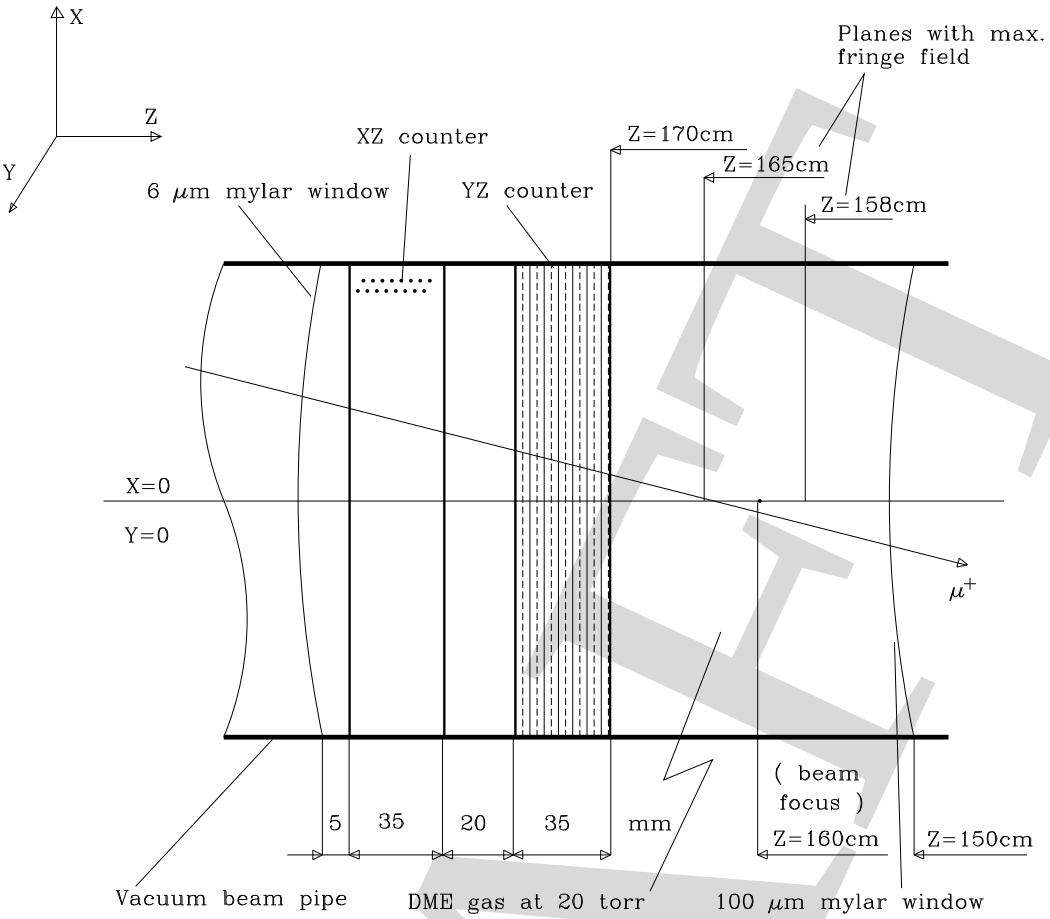

Figure 9: Sketch of time expansion chamber(TEC). Drift region is between HV3 and HV4 planes. Amplification region is between HV3 and HV2.

3 Spectrometer design requirements.

Magnet field imperfections, magnet alignment, chamber construction accuracy, chamber alignment, chamber resolution, energy loss and multiple scattering as well as any spectrometer asymmetries are all factors that will influence the significance of the E614 result. The most direct way to fulfill many of these demands is to do an accurate calibration of the component in question. A Monte Carlo of the spectrometer has been constructed and will eventually include all this calibration information as well as all of the possible interactions of the positrons with the detector.

3.1 Magnetic field.

The spectrometer magnetic field will be produced by a super-conducting solenoid with a warm bore of $\phi = 1.05$m operating at 2.2T. This large field "holds" the muon polarization when it has stopped in the target. An Oxford Magnet Technology (OMT) super-conducting coil and cryostat has been purchased for the spectrometer magnet, delivery occurring in September 1998. This coil, including the proposed return yoke have been studied using the Vector Fields Limited (VFL)[6] software routines OPERA2D and OPERA3D. The entire volume that will contain the detectors and the positron tracks of interest has been found to have a very homogeneous field that is smoothly varying, leading to the expectation that we will be able to map it to an accuracy much better than $\leq 1 \times 10^{-4}$(2 Gauss). Magnetic field influences at this level will not distort the analysis of the Michel spectrum

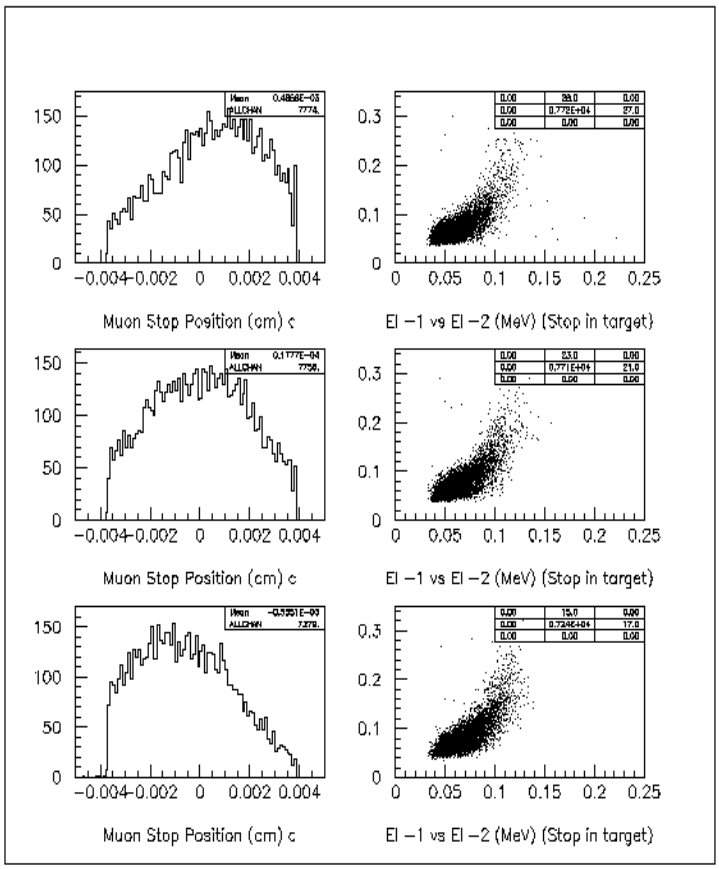

Figure 10: Stopping distribution in the target for a scintillator of thickness 320 μm (top graphs), 340 μm (middle), and 360 μm (bottom). Corresponding scatterplots show energy loss in PC(-1) and PC(-2).

significantly.

The yoke/shield for the magnet is now in the final design stages and construction will begin in the spring of 1999. Once completed the magnet will be installed in this shield and a mapping of the resulting field will be made to the accuracy described above.

A temporal instability of the spectrometer magnetic field will produce an equivalent change of the energy calibration on the same time scale. A drift at the level 10^{-4} would change the energy scale by $5keV$ at $x \to 1$ ultimately influencing the Michel parameters at a relatively insignificant level; $|\rho - 0.75| = 2.6 \cdot 10^{-5}$, $|P_\mu \xi - 1| = 1.5 \cdot 10^{-5}$, $|\delta - 0.75| = 2.7 \cdot 10^{-5}$. The field will be continuously monitored and the required level of stability will be maintained in the super-conducting magnet during the time intervals required. The solenoid will be operated in a free-running mode to minimize instabilities.

Any misalignment $\theta_{beam,B}$ between the muon beam axis and the magnetic field will be seen as a reduction of the longitudinal muon polarization $P_\mu^z = \cos\theta_{beam,B}$. Measuring the transverse component of muon polarization $P_\mu^t = \sin\theta_{beam,B}$ using ordinary μSR techniques at $B = 2T$ (muon precession period $3.5ns$) will be used to determine this misalignment. This will be done before the PDC assembly is inserted into the solenoid by inserting instead an array of scintillators. Alignment adjustments will be then made to $\leq 1mrad$ thus reducing any effect on $P_\mu \xi$ to less than 10^{-5}.

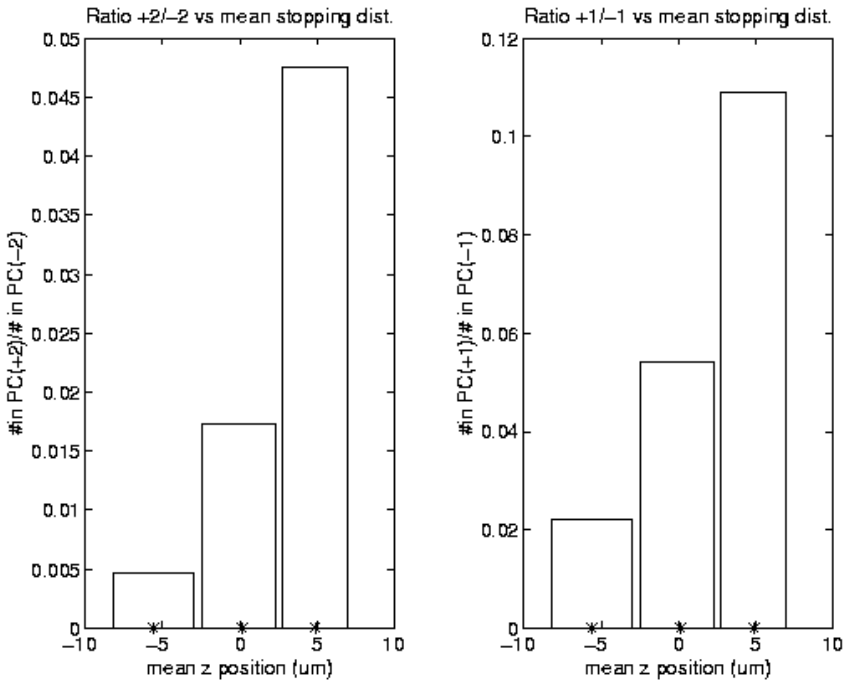

Figure 11: Graphical representation of PC ratios as a function of stopping distribution mean.

3.2 Detector requirements.

The goal of E614, a high precision determination of the Michel parameters of muon decay, requires highly exact knowledge of the energy and angular dependence of the positron spectrum. This in turn requires that the drift chambers provide high precision "hits" information on the tracks of the positrons, with high efficiency, while causing minimal disturbance to their trajectories. These demands impose restrictions on the selection of the detector materials, on the assembly accuracy, on the alignment of the detector within the spectrometer and on the readout system. Conversion of these hits to precise positions in space requires meticulous preparation and calibration of the chamber wire positions. All such demands are met in the E614 detector as will be documented below. A large list of Monte Carlo studies have been made of the detector, some of which have had substantial influence on the detector design. Several prototypes of the detector have been tested, both with radiation sources and with beams of surface muons, positrons and pions.

3.2.1 Detector materials.

The influence of the detector materials on the incoming μ have already been discussed in section 2.3. The interaction of positrons with detector materials induces changes in the trajectories through multiple scattering and reduces their energies. In the best Michel parameter experiment to date[4][5] there were $300 mg/cm^2$ of matter between the positron origin and the input window of the detector. This led to uncertainties in the derived values of the Michel parameters exceeding $4 \cdot 10^{-3}$. One obvious way to reduce these problems is put less matter in the detector, thus the E614 detector will contain approximately $15 mg/cm^2$ of matter in a similar region.

This section of the E614 detector, where the positron helix is not measured, consists of the stopping target, the PC's ± 1 or ± 2, a helium gap and the cathode foil of the first PDC. A simple response function for the Michel spectrum, taking into account only the average energy losses via

the $1/\cos\theta$ dependence has been estimated for this segment. This was done by tracking 10^9 Michel spectrum positrons, in this study employing EGS4, from their origin in the stopping target to the plane of the first PDC and fitting the resulting Michel spectrum to derive values for the Michel spectrum. The extremely simple approach of including the average energy loss of the positrons in the target, the PC's and the He gap in the response function analysis reduces the systematic shift of the Michel parameters ρ, $P_\mu\xi$ and δ to less than 10^{-3} and for η to less than 10^{-1}. The error on these estimates of the shifts however remains large, of order 6×10^{-4}, 9×10^{-3}, 3×10^{-4} and 4×10^{-2} for ρ, $P_\mu\xi$, δ and η respectively. Estimates indicate that taking into account the energy dependence of the energy loss would lead to Michel parameter correction uncertainties of: $\sigma(\rho)=\pm4.6\times10^{-5}$, $\sigma(\eta)=\pm4.0\times10^{-3}$, $\sigma(P_\mu\xi)=\pm5.9\times10^{-5}$, and $\sigma(\delta)=\pm4.9\times10^{-5}$. Fig. 12 shows that a simple linear function for the energy loss is possible for energies of Michel spectrum positrons. This correction procedure will be calibrated using the endpoint energy of the unpolarized muon decay spectrum. The above estimates appear as the uncertainties in the response function in Table 9.

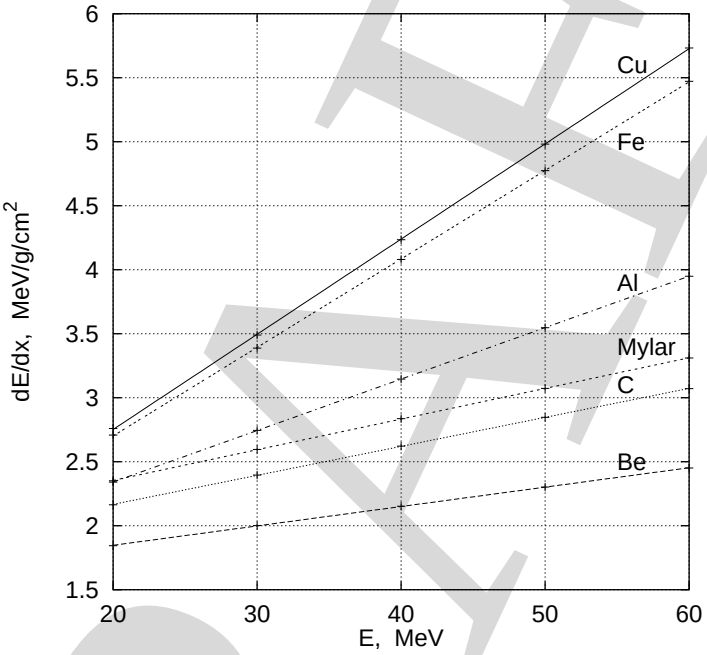

Figure 12: Stopping power for positrons in several materials.

The layout and the materials of the E614 drift chambers have been chosen to minimize the effects of multiple scattering and energy loss while providing hit information with high accuracy and efficiency. A pair of drift chamber planes (x, y) presents only 8.5×10^{-5} radiation lengths of material to a 0° track. This has been accomplished by designing the chambers to be as thin as possible while maintaining a high probability of detecting passage of the positrons. The cathode foils also serve as the gas containment foils, the sense wires are only $12\mu m$ in diameter, field wires have been eliminated and pure DME, a low Z gas, has been chosen as the drift chamber gas.

Selection of the wire material, gold plated tungsten(Re) was based on a the need to minimize scattering while maintaining strength. Elimination of the field wires was deemed to be very desirable because they would present strong scattering centers for the positrons. Although the probability of hitting a wire is only $\leq 2\%$ per PDC plane (for positron polar angles $\theta = 0°$ to 60°), hitting a wire could result in a large kink in the positron trajectory. A Monte Carlo study of the change in angle induced in a positron track by multiple scattering found a long tail that extended beyond 5°. Fig 13 shows that there is a significant difference between the number of scatterings $\geq 1.5°$ when

the chambers have or do not have field wires. For this reason the drift chambers have been designed without field wires, a successful choice as shown by the test results described below.

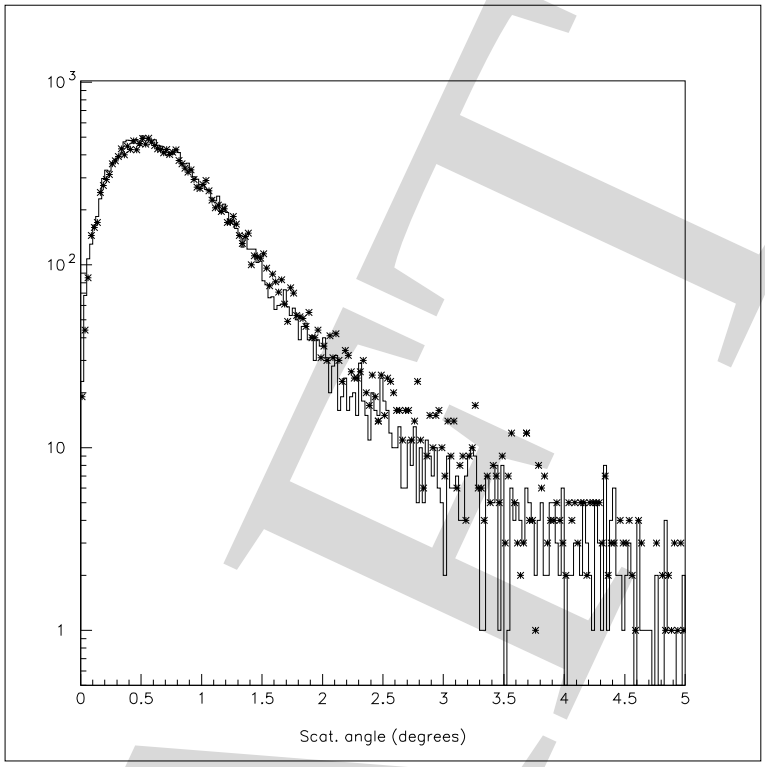

Figure 13: Scattering angle for 20 MeV/c positrons passing through five x,y chamber pairs ($\approx 24cm$) without field wires (histogram), and with field wires (stars).

The drift chamber gas, DME, has been selected largely because of its small (9° at $B = 2T$[7]) Lorentz drift angle. Even for the maximum drift angle, the drift path is increased by at most $10\mu m$. Space resolution of our PDC cell with DME gas is $\leq 100\mu m$ on average, as demonstrated in the recent prototype test described below. Errors in derived Michel parameters due to the finite value of the Lorentz drift angle are therefore very small even if we ignore it when analyzing the data.

The use of DME however imposes some requirements on temperature and pressure monitoring within the detector volume. Drift velocity of a non-saturated gas like DME depends on a temperature: $\Delta v/v = 3.5 \cdot 10^{-3}/°C$ [8]. A change in the gas temperature that we were not aware of would therefore result in a systematic shift of the distance time relation (DTR). We have simulated this effect for the E614 detector. A DTR shift $\Delta r/r < 2 \cdot 10^{-2}$ leads to shifts of the reconstructed momenta and angles of $\Delta p/p < 10^{-5}$ and $\Delta\theta < 10^{-5}$ respectively. Such small shifts cause negligible effects on the derived Michel parameters. On the other hand, the χ^2 for a reconstructed track exceeds the statistical spread when $\Delta r/r > 3 \cdot 10^{-3}$, so we need to know the gas temperature with $\sim 1°C$ precision in order to be able to account for such an increase.

The drift velocity in DME also depends on the pressure of the gas so the atmospheric pressure must also be monitored. Garfield studies indicate that this dependency is not very large in the regime in which we are operating so that if we know the atmospheric pressure to ± 1 Torr the effects will be negligible. Differential gas pressure between all volumes of the assembly must be controlled because such differences bend the cathode planes of the PDC. The Garfield routine has been used to examine the effect of such deflections and it has been determined that pressure differentials must be maintained at less than 11 mTorr. TRIUMF has experience in the design and manufacture of gas systems much larger than those of our detector with pressure stabilization at levels $\sim \pm 2mtorr$,

e.g. for Hermes, at which level cathode plane motion will not significantly influence our detector performance.

The cathode foils of the drift chambers will be $6\mu m$ thick mylar aluminized on both sides. The two aluminium layers are required in order to reduce the diffusion of He gas through these foils into the DME gas in the signal volume. Garfield studies indicate that keeping the He content in the DME at $\leq 1\%$ level will not affect the DTR significantly. A test of the diffusion rate of He gas through the proposed cathode foils showed that the rate was small, 2.5×10^{-4}cc/sec(0.015cc/min). From this result it has been estimated that a DME flow rate of ≈ 20 cc/min $\pm$ 10% will maintain the He contamination in the DME at about 0.1% $\pm$ .01%. Garfield simulations of DME-He gas mixtures indicate that a 1% change in He levels will cause a 1% change in drift times so that our system should maintain drift time stability to 10^{-4}. The gas handling system will be designed to provide such a flow rate. A recycling system will be installed if the economics justifies it.

There is, because of the E614 detector geometry, a technique available to minimize the influence of matter on the derived parameter values. The positron energy loss in the E614 detector is given by $\Delta E(E,\theta) = \Delta E(E,\theta=0)/\cos\theta$, where θ is the polar angle with respect to the magnetic field and E is the positron energy. This formula expresses the fact that the effective thickness of the detector material (path length) grows with the θ. The $1/\cos\theta$ dependence for the planar target, for the planar gas gaps and for the planar cathode plane foils is obvious, but it also applies to the wires even though the energy loss does not have this simple dependence on θ (for cylindrical wires) because the probability of hitting a wire does have such a dependence on θ. This means, that the $1/\cos\theta$ dependence is essentially correct for all materials within the detector volume.

3.2.2 Detector assembly precision.

The E614 detector assembly procedure has been worked out with great care in order to avoid cumulative errors that could have a large influence on the response function and the energy calibration of the detector and consequently on the derived Michel parameters. For example, accumulation of $2\mu m$ repetative positioning errors in the wire plane spacings or in the positioning of the wires within the chamber planes could result in Michel parameter shifts at the 10^{-4} level. The prevention of accumulative errors at this level during the chamber assembly is assured by the high precision manufacture of the chamber components and of the apparatus used in the assembly. The accuracy required for the positioning of individual wires is not quite so demanding, random errors at the level $\sigma \leq 20\mu m$ have been found with Monte Carlo studies to produce negligible effects on the Michel parameter determination. Several groups have previously achieved construction accuracies similar to these[9],[10].

The design of the E614 detector and the assembly procedure are such that there will not be a need for microscopic adjustments after construction since all distances are predefined by the high precision manufacture of each element. Half of the detector array is shown schematically in Fig.2. The E614 chamber planes, both for the PC's and for the PDC's are each manufactured separately and then assembled into the stack which forms the detector shown in this figure. The basic piece of both the PC's and the PDC's is a circular plate glass frame of thickness $3.2(\pm 0.0, 0.1)mm$ with an outer diameter of $600(\pm 0.5)mm$ and an inner hole of diameter $400(\pm 0.02)mm$. In addition there are four alignment holes with diameters of $52(\pm 0.1)mm$ and centers which are $45° \pm 10'$ from each other at a radius of $26cm$ from the center of the plate. The surface of these plates is flat to $0.01mm$. A G10 based "lamel" on which there are strips of copper for making connections to the wires is glued by epoxy onto this glass frame. Thin translucent glass ceramic(CITAL) rings with $32(\pm 0.02)mm$ and $50(\pm 0.1)mm$ innner and outer diameters respectively are glued into four $52mm$ diameter alignment holes in the frame, the distance between these rings being maintained from glass frame to glass frame by use of a single gluing stand. These rings function as very high precision "posts", their $4(\pm 0.0005)mm$

thickness determining the distance between nearest chamber planes. The low thermal expansion coefficient of these rings (3×10^{-7}inch/inch/°C) guarentees that this spacing will be independent of the temperature of the detector environment. The prepared frame is then put on a winding tool.

Another glass plate is the basis of the winding tool. One face of this plate has been determined to be flat to better than $0.3\mu m$ using an interferometer (with the plate in the vertical position in order to eliminate gravitational sag). Four $340mm$ long, $15mm$ wide glass rulers are put on this flat surface of the plate in optical contact with the surface so that less than one Newton ring ($0.3\mu m$) is visible between both surfaces. These rulers have 330 diamond cut grooves into which the sense wires are put, thus defining the distance between the wires as that between the grooves. The grooves, $13mm$ long, extend from one edge to $2mm$ from the other and are at 90 degrees to the latter with a tolerance of ±30 arc seconds. They are $15 \pm 5\mu m$ wide and not less than $5\mu m$ deep. The statistical fluctuation of the groove positions on the rulers is $\sigma = 1.5\mu m$ and the accumulated error is less than $1\mu m$ across the $350mm$ of the chamber plane. The wire positions with respect to the winding tool plane is defined by the thickness, $4 \pm 0.0005mm$ of the rulers. The four rulers are put on the winding tool surface with $90° \pm 1''$ between the nearest rulers using the grooves on an octagonal glass frame. Following this, 65 small disks of thickness $1.997 \pm 0.0005mm$ are placed on the surface of the winding tool evenly spaced along a circle of diameter $380mm$. These disks define the position of the $6\mu m$ thick double sided aluminized mylar cathode plane relative to the surface of the rulers, i.e. the wires.

In order to eliminate any gravitational sag, the winding tool and the PDC frames are hung vertically on a steel strip with a felt gasket. The PDC frame is pressed to the tool surface until optical contact is established between the 4 CITAL posts and this surface and then fastened in place. The side on which the lamel is glued is next to the winding tool surface. A cathode plane, its position relative to the tool surface and consequently to the alignment faces of the 4 posts fixed by the 65 small disks described above, is then glued onto the PDC frame, a conductive glue providing electrical contact between the cathode plane and the appropriate location on the lamel. Once the glue has dried the plate is turned over so that the lamel surface is now accessible and again pressed to the tool surface so that optical contact is established between the other ends of the 4 CITAL posts and this surface. The wires are then wound between two opposing rulers. The wires are fixed at both ends by the threads of the two diametrically opposite screws, the $1 \pm 0.005mm$ thread spacing providing a preliminary location of the wire positions. The screws can be moved along their axes by additional micro-screws. The wires, once located within the grooves of the ruler as observed through a microscope, are fixed in that position even if the screws are moved $\pm0.3mm$ Once the wires are in their correct positions they are glued to the lamel by epoxy and then put in contact with the traces on the lamel with conductive glue. A second glass plate is mounted on the winding tool, a cathode foil glued in place and then wires are wound between the set of rulers at right angles to the first set. A third glass plate is then equipped with a cathode foil. These three glass plates are then pressed together to form an x,y chamber consisting of a cathode foil that also functions as a gas containing foil, a plane of wires, another foil followed by a set of wires at right angles to the first and finally the other gas containing cathode foil. The spacing between the foils and the wires are all established by the 4 CITAL posts. The 40 and $60mm \pm 0.0005mm$ helium gaps between these x,y pairs of PDC's are provided by appropriate combinations of CITAL rings of 20 and $40mm$ thicknesses. These CITAL spacers are glued in G10 rings of similar structure to the glass rings. These G10 rings, which are of a larger outer radius, function as the supports for the preamp mother boards and form a part of the gas barrier between the DME in the chambers and the He gas in the gaps.

The final detector assembly is clamped by four screws inserted through the CITAL "beam" that is formed by the back to back assembly of the CITAL posts of the chamber planes and the CITAL spacer rings. These four posts are the support structure of the detector. Tests and analysis were carried out at the Civil Engineering Department of the University of British Columbia to predict the behavior of this proposed support structure design. Material properties of CITAL CO-115M were

determined and analytical predictions of support structure behavior were performed.

For a brittle material, such as CITAL CO-115M, the compresssion strength results are dependent on the load apparatus and the specimen dimensions. A certain amount of variation in strength is to be expected depending on the particular application. The maximum load reached in the tests, 37.1kN(32.0 MPa), produced no failures. This strength is well above the design stress maximums. No apparent permanent deformation was observed at this level of loading. The derived value of the CITAL elastic modulus is 57.0 GPa and its maximum strength in compression is about 900 MPa.

Friction between the finished surfaces of adjacent segments of the CITAL beam was not determined. Experiments aimed at determining load-slip behavior of the friction surfaces resulted in fracture of the beam segments at loads far in excess (400kg/5kg) of those that will occur in practice without ever observing slip between ajacent segments.

A single full scale, 1.06 m long CITAL beam was tested for deflection under load with the ends simply-supported. These tests were made for a variety of load cases. Computer analysis was also made to predict behavior for two extreme end-support conditions: simply-supported (point supported at ends) and fixed-fixed(supported so that rotations of the ends is not possible). The analysis determined that the expected range of stresses and mid-span deflection for the $1.06m$ long four-beam structure carrying 4 kg per load plane are:

	Simply-Supported	Fixed-Fixed
Minimum Required Axial Stress (MPa)	0.55 - 34.0	0.35 - 23.0
Mid-span Deflection (μm)	39 - 2500	0.8 - 500

The large range is due to the unknown amount of rigidity provided by the G10 and glass plates which link the four beams together. If there is no rigidity, then each beam behaves independently and the higher values result. The best case, therefore, is the fixed-fixed condition with very rigid links between the beams. Although the minimum axial stress is quite low for the 'best case', it is recommended that at least 20 MPa be provided.

Recommendations from this study are:

- The minimal axial pre-stress in each beam should be 20 MPa but should not exceed 50 MPa. This stress will cause and axial shortening of each beam of about $400\mu m$.
- One segment with a calibrated strain guage chould be used in each beam to determine the level of pre-stressing. A torque wrench used during the experiments was not as accurate as the instrumented section. This guage will allow for long-term monitoring of the axial stress in each beam.
- Care must be taken during assembly to prevent the beams from being accidentally overloaded.
- The four beam structure should have end constraints which prevent end rotations in order to approach the fixed-fixed support condition. In this case, assuming the glass and G10 links between the beams are relatively rigid, the maximum mid-span deflection, if the beam is loaded symmetrically with 4kg loads placed at the locations indicated on the working drawings (Fig 2), is limited to less than $1\mu m$.

The quality of the chamber components will be monitored as they are assembled.

The first pieces assembled are the cathode foils which also serve as the gas envelope for the DME of the chambers. A special device, shown schematically in Fig 14 will be manufactured for this purpose. The gas outlet pipe is closed and gas is fed into the inlet pipe at a fixed rate. The rate at which the internal pressure rises is related to the tension of the foil. Once the pressure reaches a predetermined level the gas flow will be terminated, the rate of pressure loss will then be monitored

as a measure of the leakage of gas from the enclosed volume. The results will be used to accept or reject the foils. The same device will be used to test the integrity of the glue joint between the foil G10 and the glass rings.

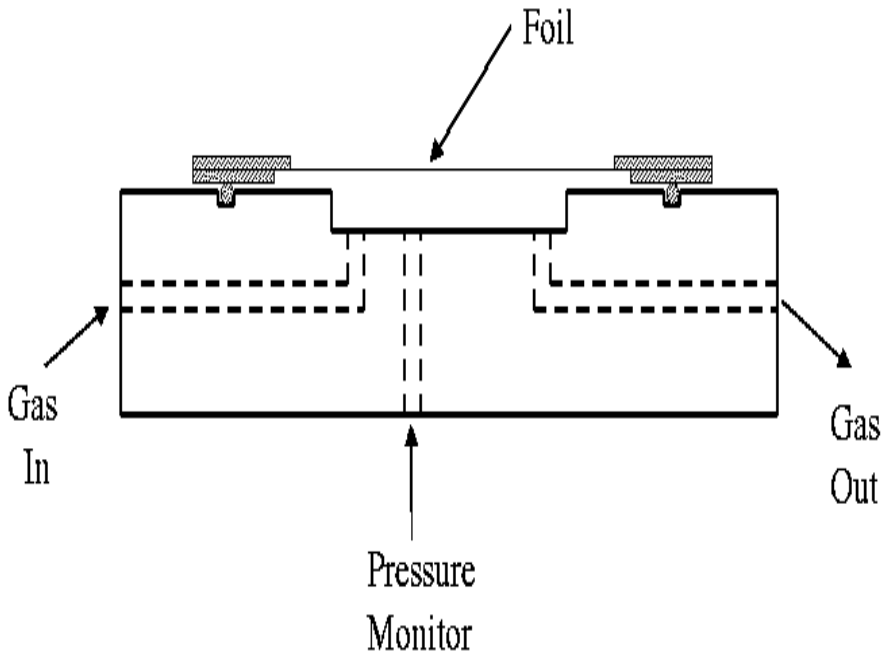

Figure 14: Schematic of tension and leak-rate testing.

The wires will then be strung on the accepted glass ring, foil assemblies. The tension in the wires will be tested using a purchased wire resonance meter. Note that this will also be a test for the wire continuity. The wire positions will be measured with a pair of traveling microscopes equipped with a video cameras and digital readouts. The relative wire positions will be logged. Any wires that do not have the correct tension or are too far from their correct relative positions will be replaced using these traveling microscopes.

The completed foil and wire assemblies will then be assembled into xy pairs. These xy chambers will then be tested for their ability to hold voltage and subsequently tested with sources and possibly with beam to assure that they meet requirements.

The influence of systematic deviations of the PDC assembly from the ideal has been studied using Monte Carlo vacuum helices(energy loss and multiple scattering turned off) for $p_{e^+} = 50MeV/c$ over angular range $10 - 60°$. Chamber hits were generated for wire plane spacings of $4mm + \beta$. The resulting helices were reconstructed assuming $\beta = 0$. The results indicated that for $\beta = 2\mu m$ there would be an energy calibration shift of $\Delta p_0 = 10keV/c$. Such an error would produce the following shifts of Michel parameters: $|\rho - 0.75| = 5.2 \cdot 10^{-5}$, $|P_\mu \xi - 1| = 3 \cdot 10^{-5}$, $|\delta - 0.75| = 5.4 \cdot 10^{-5}$. There are 78 wire planes and 18 helium gaps for a total of 96, meaning that the accumulated error from a recurring $2\mu m$ mistake would total $192\mu m$. The total length of the assembly can be determined with optical techniques to $\approx 50\mu m$ assuring that errors this large will not be unknown so that the Michel parameter shifts estimated here (and entered in Table 9) must be considered as upper limits. In addition the position of each sense wire in PDC assembly will be measured using cosmic rays and beam particles.

The influence of random errors in wire positions (without systematic errors) on the Michel pa-

rameters was also studied by Monte Carlo again using vacuum helices simulated for ideal sense wire positioning. The wire positions were randomized with a standard deviation σ and the helices were reconstructed for these new wire positions. For $\sigma \leq 20\mu m$ the resulting shift in the derived momentum was $|\Delta p| < 1keV/c$ and in the measured angle was $|\Delta\theta| < 6 \cdot 10^{-4}$. Such small effects will cause negligible shifts in the Michel parameters. Wire position measurements to this accuracy have been achieved in our prototype tests.

3.2.3 Detector alignment.

A misalignment $\theta_{PDC,B}$ between the PDC assembly and the magnet axis would distort the Michel spectrum. The Michel spectrum is independent of the azimuthal angle ϕ, but such a misalignment $\theta_{PDC,B} \neq 0$ would introduce a ϕ dependence into the measured spectrum. With total statistics of 10^8 muon decays this artificial ϕ asymmetry will be measurable to an angular accuracy of $0.1mrad$. Corrective adjustments will then be made and a parameter will be introduced into the analysis to account for any remaining misalignment. Shifts of the Michel parameters, because of a misalignment at a level not accounted for in this manner, will be negligible.

3.2.4 Detector geometry.

The geometry of the original(baseline) detector had equal, $4.8cm$, center to center spacings of the PDC pairs(x, y). This geometry presents the possibility that the wavelengths of certain helical tracks would coincide with the period of the chamber pairs, thus producing poor fits in the x or y projection. A Monte Carlo study was therefore made of alternating these spaces such that the distances between the center of each pair was either 4.8 or $6.8cm$. It was found that this change substantially improved the momentum resolution (see Fig. 15) by increasing the lever arm over which the track position is measured. Little difference was found in the angular resolution for the two cases. The detector will be assembled with spaces between pairs that are not all identical and on average that are larger than the baseline design.

3.2.5 Detector acceptance.

The geometric acceptance of the E614 spectrometer as a function of θ and E_{e^+} has been studied with the GEANT Monte Carlo for angles from 5° to 85° and for momenta from 6 MeV/c to 70 MeV/c. The 70 MeV/c momentum being included to study the acceptance of positrons from pion decay. For each angle and energy 10^4 events were generated and for the central regions no more than one event was lost, the acceptance thus being unity to better than 1 part in 10^4 for angles from 5° to 75° for momenta from 20 MeV/c ($\approx$ x=0.3) to 52 MeV/c. It must be mentioned that the acceptance results were derived using the very restrictive requirement that the particle traverse all the chambers in its direction of travel in a limited number of steps in the GEANT routine. Test runs for the large angle, low energy points in which these restrictions were relaxed did produce more "acceptance". Despite regions where positrons are lost via multiple scattering and energy loss, the nominal acceptance is very uniform and very close to unity, better than 1 part in 10^4. This excellent geometrical acceptance of the E614 detector simplifies the understanding of any losses to that of understanding of physical effects such as energy loss, multiple scattering, etc. In the actual experiment the trigger will examine any positron track following a muon stop and even if the positron does not travel to the end of the detector system it may prove to be possible to analyze such events and thus extend the usable θ and momentum regions.

The effects of inefficiency, not accounted for in the above study, are expected to be small because the detector has an abundance of planes. The main tracking detector has eight x, y pairs that are fully instrumented. In addition there is a dense stack of 6 PDC planes that serve to aid in analysis

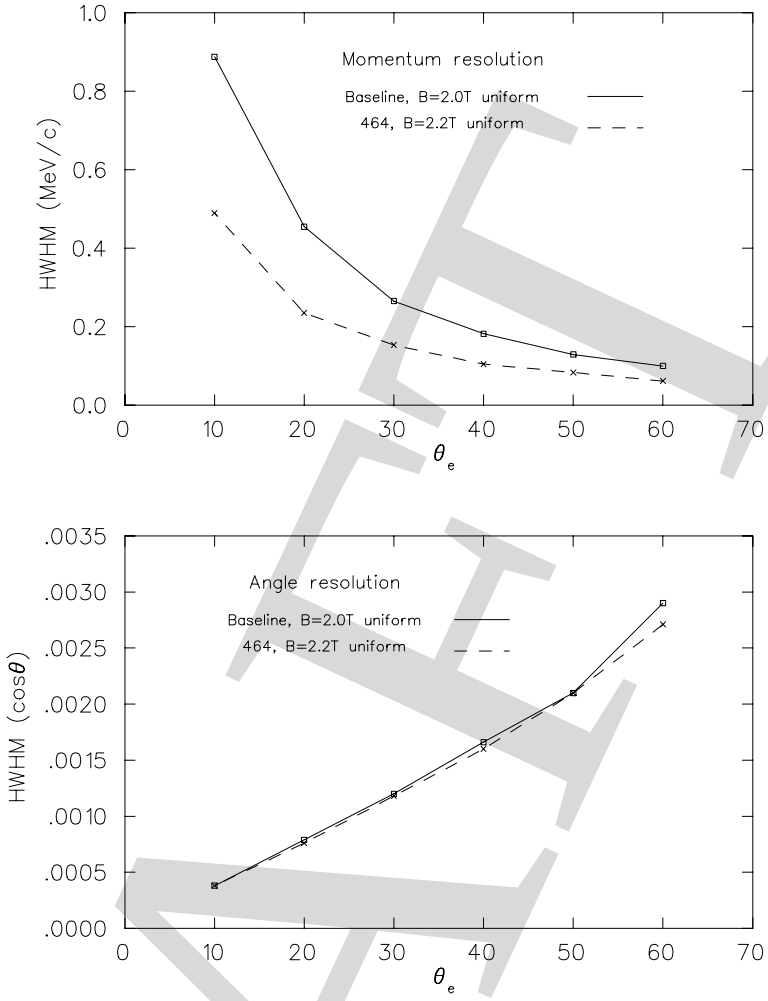

Figure 15: Top: momentum resolution for the baseline spectrometer (solid line), and spectrometer modified to include alternating 4.8 and 6.8 center to center spaces(464 option, dashed line). Bottom: angle resolution for the same two options.

of small radius helices(see Fig. 2. Present plans call for instrumenting only the center 48 wires of these 6 planes. All wires will be installed on the planes in this dense stack so that if we determine, in studies presently under way, that more of these wires need to be instrumented to enhance efficiencies, it will be possible. The individual PDC cell efficiency is high and will be higher for tracks that are at a sufficient angle to miss the dense stack but the studies are aimed at determining that there is no potential for an angle dependent efficiency being introduced by not fully instrumenting the dense stack.

There are several technical reasons why individual wires in the PDC's may have low efficiency. There are 22 PDC planes through which the positron track passes (if no annihilation or other violent loss occurs, $\leq 10^{-5}$) and since far fewer points than this will be required to fit the positron helix modest inefficiencies can be tolerated and still result in an over-determination of the helix.

Inefficiencies may result for several reasons related to the passage of the incoming μ through the upstream chambers. The first problem arises because the energy deposited by a muon in a PDC cell can be $5 \div 20$ times larger than by a positron. This can result in a saturation of the preamps and hence - to a long recovery time. Tests using VTX preamps [11] (which have a gain of $1mV/fC$, a dynamic range of $400mV$ and a saturation output voltage of $1V$) made during the PDC test runs showed that the total gain (wire+preamp) was about $10mV/1e$. This means that the muon may not

saturate these preamps (about 60e for the 4mm gap). The second problem arises from the possibility of confusing muon hits for those of a decay positron that is going upstream. In offline analysis the introduction of a $500ns$ wait time after the muon arrival before any positron hits are analyzed will lower the probability of making this mistake by a factor of ≈ 20. The third problem arises because of the long dead time ($> 20\mu s$) of a sense wire due to the slow dissipation of the ion cloud around the hit sense wire. The dead zone along the sense wire is about $0.5mm$. The influence of these three effects on track reconstruction will be similar to that for inefficient wires and will be accounted for by the redundancy in available hits. We will fine tune and verify our ability to reconstruct intermingled tracks by studing beam positrons that are near in time ($\sim$2 positrons will be available in each of our $10\mu sec$ windows) but in random coincidence with the beam muon that triggered the spectrometer.

3.2.6 Detector resolution.

There are many effects that enter into the resolution of the drift chambers(PDC). The influences of multiple scattering, energy loss and drift gas properties were described above in subsubsection 3.2.1 where we discussed detector materials. The influence of the accuracy of the detector assembly was discussed in subsubsection 3.2.2. The influence of timing resolution, time shifts, position and energy resolution, and the detector calibration will now be discussed.

In the reconstruction of events detected by the E614 detector an uncertainty in the zero time(t_0) used for the drift chamber time to distance conversion will influence the momentum(p) and angle(θ) resolution. Examination of this effect was carried out by fitting several thousand helices simulated with a Gaussian distributed error on the radial distance from the PDC wires (Δr) which had a standard deviation equivalent to a t_0 jitter of $\approx 5ns$. This study has shown that for $0.4 < x < 0.95$, $0.5 < \theta < 0.985$, the effect on the determination of the momentum and angle were:

$$\begin{aligned} \Delta p &\ll 1keV, \\ \Delta\theta &\ll 10^{-4} degree, \\ \sigma(p) &\approx 80keV, \\ \sigma(\theta) &\approx 10^{-2} degree. \end{aligned}$$

The determination of t_0 in real data was examined for the prototype chamber test discussed below where it is required for each wire in the chamber. The method employed for doing this was to start by finding the peak, N_p, near the minimum time in the TDC spectrum (maximum channel # in common stop mode) and assuming that t_0 is the TDC time corresponding to fN_p, where f is some fraction (chosen to give a good first guess). This was followed by several iterations to fine tune the value of t_0 using tracking information. For this data set it was found that the variations of t_0 from wire to wire within the same plane was small so that initial guesses for all wires in a plane were essentially the same. The iterative procedure resulted in determinations of t_0 to approximately a single TDC channel ($\pm 1ns$). This is a higher accuracy than the uncertainty examined here so even the small errors listed above are overestimates, leading to the conclusion that the determination of t_0 will have a negligible effect on the determination of the Michel parameters.

A shift in t_0 could also result in derived Michel parameter shifts. Such an effect was simulated with the approach described above for t_0 jitter influences, with one difference - the error on the distance from the PDC wires was fixed and the same for all helices. The shifts Δp and $\Delta\theta$ grow, as does the χ^2 of the fit as Δr increases. They reach $\Delta p = 1.4keV$ and $\Delta\theta = -0.0022°$ for $\Delta r = 20\mu m$ (corresponding to $1ns$ t_0 shift). Such shifts correspond to less than $5 \cdot 10^{-5}$ shifts of the Michel parameters.

The effect of the position resolution of the drift chambers has been studied with Monte Carlo simulations. A straightforward analysis for a position resolution of $\leq 100\mu m$ results in an energy resolution of 450 keV and an angular resolution of 0.4° over most of the spectrometer acceptance(see

results for baseline detector in Fig 15). These values will be improved by employing the alternating 464 He gaps scheme discussed in section 3.2.4. Still further improvement will be achieved using more sophisticated reconstruction techniques than those employed in these studies. It was also found that energy resolutions of ≤ 100 keV, folded into the Michel spectrum, had no influence on the derived values of the Michel parameters hence the experimental energy resolution will not affect the final results as long as it is determined to this level of accuracy.

The accuracy of the calibration of the detector will of course influence the results. Such aspects as the location of the wires, the energy and angular resolution, the determination of the energy scale and the energy and angular acceptance of the detector will all be determined in special systematics studies. The beam time requirements laid out in Table 7 show that a large fraction of the data taken by E614 will be for this purpose.

The wire positions within the E614 detector assembly will be checked with various measurement techniques, notably the traveling microscopes during manufacture. The wire positions finally will be determined with cosmic rays and beam particles. Our prototype test results indicate that these positions will be determined to better than the $\pm 20 \mu m$ that our Monte Carlo studies(see section 3.2.2) indicate will result in negligible influences on the derived Michel Parameters.

A spectrum will be accumulated for the decay of a sample of muons that are unpolarized. This spectrum will provide an x=1 (end-point energy) calibration for both directions in the detector.

To study the influence of an energy calibration error, Δ on the Michel parameters a Michel spectrum was generated with the substitution $x \rightarrow x + \Delta/E_{max}$, where x is the reduced positron energy ($x = 1 \rightarrow E_{max} = 52.831 MeV$). This spectrum was randomized according to total statistics 10^{11} $\mu \rightarrow e$ decay events in a 4π solid angle. The large statistical sample was employed to be certain that the results were dependent only on the energy calibration error. This spectrum was then fit by an undistorted Michel spectrum (with $\Delta \equiv 0$). The result is that deviations of the Michel parameters grow linearly with $|\Delta|$. For $|\Delta| = 10 keV$ they amount to $|\rho - 0.75| = 5.2 \cdot 10^{-5}$, $|P_\mu \xi - 1| = 3.0 \cdot 10^{-5}$, $|\delta - 0.75| = 5.4 \cdot 10^{-5}$. These numbers are listed in Table 9 for the positron energy calibration error. Note that these numbers are equal to the correction required for an error of $\sim 200 \mu m$ in the length of the detector and to twice that required for a 2 Gauss change in the magnetic field (sections 3.2.2 and 3.1 respectively). This results because both these effects are equivalent to energy calibration shifts, $10 keV$ and $5 keV$ respectively.

To demonstrate that the calibration of the end point of the energy spectrum can be determined to order $5 keV$ we have done reconstruction studies with a global fit (treating the helix as an unbroken function) using a "sliding" technique. In this procedure the positron helix, as generated by the EGS4 Monte carlo, was fit sequentially using subsets of four x, y PDC pairs, thus in Fig. 2 the first such pair, moving out from the stopping target, is chamber *1*, the second is chamber *2* etc. The subsets consist of *1234, 2345, 3456, 4567*, and *5678*, each such subset being referred to as a *slide*. The fit results are retained (selected) for the slide with the maximum confidence level value (χ^2 is not used for the selection because the number of wire hits in slides varies from slide to slide). This technique will select the positron track segment that is most free of substantial kinks due to large energy loss and/or scattering events. The total event statistics will be distributed among the 5 slides.

It was found that for the sliding technique the baseline spectrometer energy resolution became worse at small angles, particularly for $\theta < 20°$ while the angular ($\cos\theta$) resolution becomes better at these angles, in excellent agreement with the GEANT results shown in Fig. 15 for the same version of the spectrometer. Since the Michel spectrum is a function of E and $\cos\theta$, the resolutions for both are important for determination of the Michel parameters, but from our studies a good energy resolution is more important than a good angular resolution, especially, close to the positron maximum energy, $x = 1$. Several techniques suggest themselves for the improvement of the energy resolution at small angles, for example one could increase the number of planes employed in the slides, increase of the helium gap between the PDC's, i.e. lengthen the detector, or employ the slide technique to find kinks

and then fit "through" these kinks employing many more planes. Employing five rather than four x, y PDC pairs in a slide does improve the energy resolution at small angles and will be considered for the analysis of the real data. Fig. 15 shows that significantly better small angle energy resolution does result from increasing every other helium gap length. The technique of fitting "through kinks" has not yet been studied. It is also possible that better energy and angular resolution will be achieved through use of the Kalman filtering technique[12] which takes into account multiple scattering effects. G.Lutz[13], for example, gained a factor of 2 in the momentum resolution of a detector using the Kalman technique.

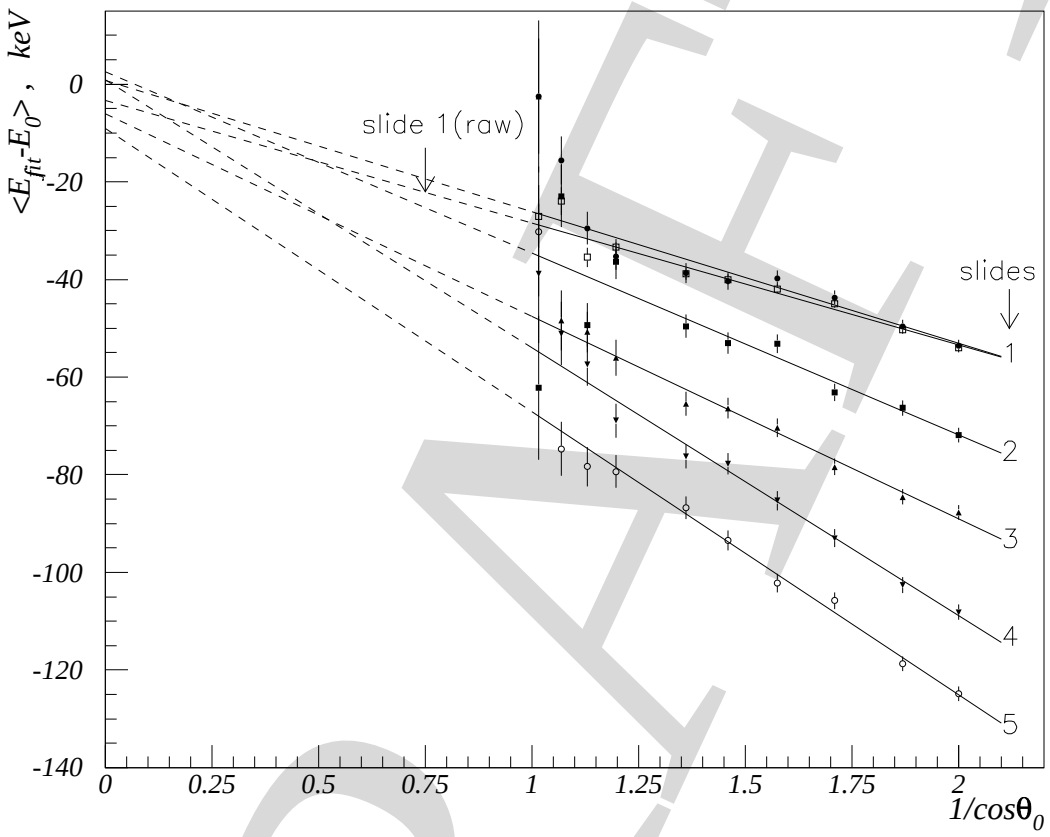

Figure 16: Mean reconstructed positron energy $\overline{E_{fit}}$ as a function of $1/\cos\theta$. $E_0 = 50MeV$, $\sigma_{PDC} = 50\mu m$. Straight lines are the fits with function $\overline{E_{fit}} = E_0 - \alpha/\cos\theta$.

Fig. 16 shows the dependence of the mean reconstructed positron energy $\overline{E_{fit}}$ on $1/cos\theta$ for E_0=50 MeV/c, again assuming σ_{PDC}=50 μm. One can see that it can be parametrized with a linear function $\overline{E_{fit}} = E_0 - \alpha/\cos\theta$, where E_0 is the initial (50MeV) positron energy and α is the energy loss of a $cos\theta$=1 positron track before entering the selected slide. Straight line fits to each of the slide data points, presented on Fig. 16 show that for, $1/\cos\theta = 0$, $\Delta = \overline{E_{fit}} - E_0 = (-2.2 \pm 2)keV$, Similarly at $\overline{E} = E_0 - \alpha/\cos\theta$ dependence at $E_0 = 20MeV$ the result was $\Delta = (-2 \pm 1)keV$.

The above procedure, fitting straight lines to the $1/cos\theta$ dependence of positron tracks reconstructed with the sliding technique, was repeated to study the $x \to 1$ positron edge. Employing $2 \cdot 10^5$ positrons generated by EGS4 for initial energies and angles in the ranges $0.9 < x \leq 1$ and $0.4 < \cos\theta_0 < 0.995$ resulted in the five energy points shown in Fig. 17, one for each slide. The average is $\overline{E_{max}} = (52.77 \pm 0.03)MeV$, very close to the correct value $52.831MeV$. The conclusion is that the planar geometry of the E614 detector makes it possible to calibrate the energy scale with high precision. A higher statistics ($2 \cdot 10^7$ events) study would be expected to provide an energy cali-

bration with an accuracy better than $4keV$. Again taking a conservative approach we have assumed that the energy calibration uncertainty will be $\sim 10keV$, and thus have inserted, in Table 9, the shifts found for such an energy error as the uncertainty in the Michel parameters. These numbers were derived in section 3.2.2 where we were studying the influence of cumulative errors in the plane positions.

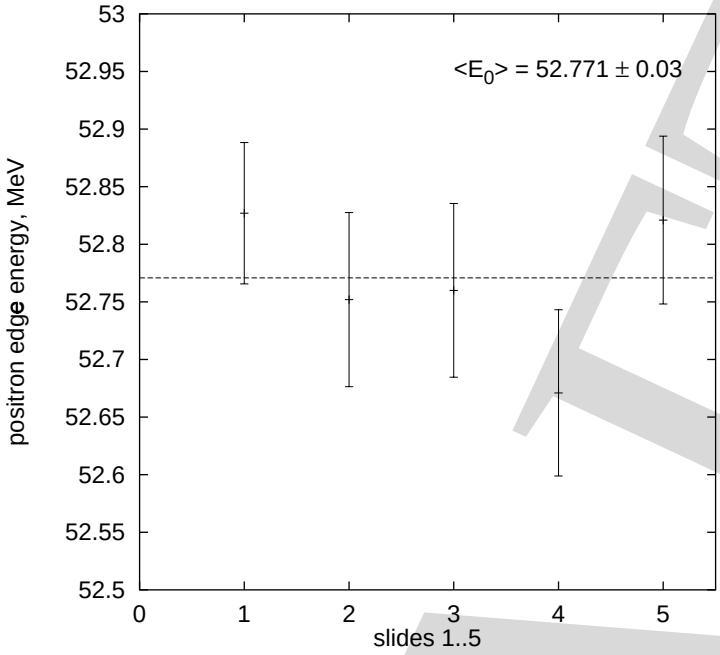

Figure 17: Result of positron edge fit for all slides. Initial spectrum in target was uniform in energy and $\cos\theta_0$ in the range $0.9 < x < 1$, $0.4 < \cos\theta_0 < 0.995$. Total statistics $2 \cdot 10^5$ events.

The energy calibration will not be restricted to this $x \to 1$ point but can be assumed to apply over the full energy range $0.4 < x < 1$ since the E614 detector is a linear detection system because of the homogeneous magnetic field. This latter point can be verified using the idea suggested by M.Cooper which utilizes the fact that the ratio

$$M = \frac{\frac{\partial}{\partial x}\left(d^2N(x = 0.75, P_\mu\xi = 0)/dx d\cos\theta\right)}{d^2N(x = 0.75, P_\mu\xi = 0)/dx d\cos\theta} = \frac{16}{9}$$

is essentially independent of the Michel parameters, ρ, η, $P_\mu\xi$, and δ. Here $d^2N/dx d\cos\theta$ is the differential muon decay rate spectrum for unpolarized muons. A simple estimate shows that $P_\mu\xi$ need not be exactly zero for this calibration to be applicable, for example if $P_\mu\xi = 0.01$ the errors on the experimental values of ρ, η, $P_\mu\xi$, δ change this ratio by less than 10^{-7},$1.7 \cdot 10^{-5}$, 10^{-7}, 10^{-7} respectively. An energy calibration error $\Delta \neq 0$ results in $M = \frac{16}{9}(1 - \Delta/E_{max})$.

The equality of the acceptance and the relative efficiency of the forward and backward sections of the detector will influence the determination of the Michel parameters, particularly $P_\mu\xi$ and δ. The spectra in these sections of the detector that are measured with the unpolarized muon sample will be used to determine these relative factors. The equality of ρ measured in the backward direction compared with that for the forward direction will provide the relative efficiency of the upstream/downstream PDC assembly. This unpolarized spectrum measurement will require about 90 days at $150\mu A$.

3.3 Chamber Tests

3.3.1 Prototype test in a magnetic field.

Tests have been performed on 1:4 scale prototypes of the PC and PDC detectors to examine timing characteristics, position resolution and efficiency in a high magnetic field. These tests were performed in the TRIUMF M15 beam line at $p = 35MeV/c$ which had about 98% positrons and about 2% positive muons. The beam diameter was more than $10mm$(FWHM) so that its distribution density within any $2mm$ PC cell was essentially flat. The PC prototype assembly is shown in Fig. 18.

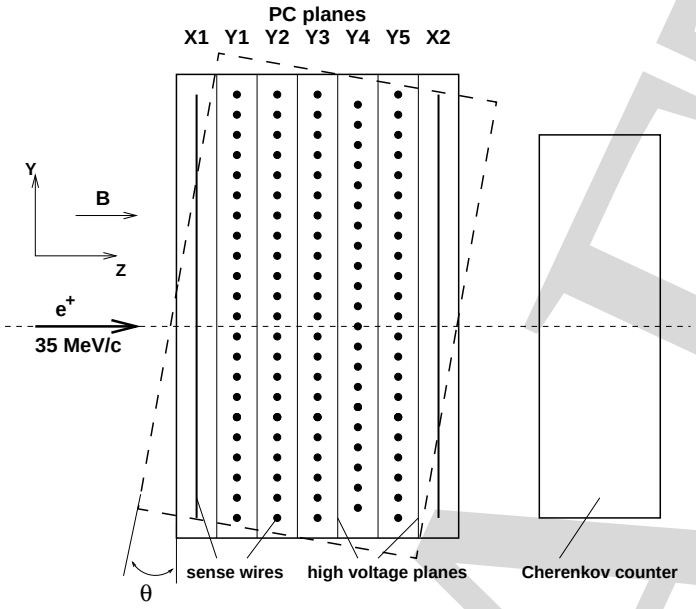

Figure 18: Schematic of the experimental setup. Sense wires in $Y4$ plane are shifted by $1mm$ along Y-axis with respect to all other Y planes. It was possible to rotate PC assembly in YZ plane in the range of angles $\theta = 0 \div 60°$. The dashed line contour on the figure represents the PC assembly rotated by 10°.

In the PC prototype assembly the sense wire positions along the Y-axis in planes $Y2$ and $Y3$ were identical while those in $Y4$ plane were shifted by $1mm$ along Y-axis with respect to $Y2$ and $Y3$. Signals from $X1$, $Y1$, $Y5$ and $X2$ planes were used as a trigger indicating that a particle had passed through these planes and the responses of planes $Y2, Y3, Y4$ were studied. The tests were made using the *HELIOS* super-conducting magnet of the TRIUMF μSR Facility to provide magnetic fields up to $6T$. Positrons were identified by the Cherenkov counter (see Fig. 18). It was possible to rotate the chamber assembly in the YZ plane up to $\theta \leq 60°$ as shown by a dashed line contour on Fig. 18.

The measured drift time spectra for several magnetic field settings appear in Fig. 19 where (a) is for signals from individual sense wires and (b), (c) and (d) are for sum signals from the identified planes. The RMS and center of gravity of these drift time spectra were calculated for angles of incidence from $0° \rightarrow 60°$. The Y2+Y3+Y4 combination was found to have a mean time jitter of $2.5ns(RMS)$ at $B = 2T$. The efficiency of these chambers for positrons was found to be good independent of the magnetic field indicating that their efficiency for muons will be excellent.

The PDC prototype assembly and study was essentially identical to those of the above described PC prototype assembly. Again the tests were done on the M15 beam line at $p = 35MeV/c$. The efficiency of the PDC's was found to be better than 99% with DME(dimethyl ether) as the drift gas. The resolution of the prototype PDC, σ_{PDC} at $B = 0$ measured mean value was $48\mu m$ at $\theta = 0$ and grew to $64\mu m$ at $\theta = 60°$.

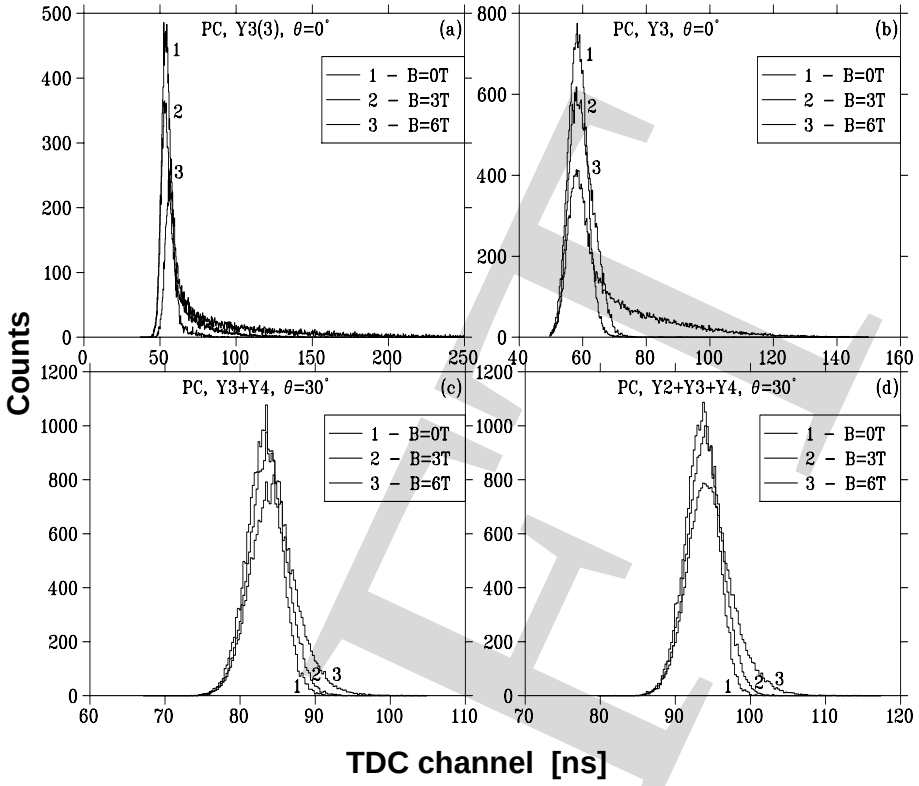

Figure 19: Measured PC drift time spectra at $U = 1980V$ for *Y3(3)* wire (a), *Y3* plane (b), *Y3+Y4* planes (c) and *Y2+Y3+Y4* planes (d). All spectra are normalized to equal total counts.

3.3.2 Full scale prototype tests.

Full scale prototype planar drift chambers(PDC), without field wires were built and tested. For this test seven planes were manufactured and assembled into an array of 2 planes measuring the y position and 5 measuring the x position of the passing particles, a similar arrangement to that shown in Fig. 18. The tests were done on the bench using an ^{55}Fe source and in M13 employing minimum ionizing high energy pions and highly ionizing surface muons. The data was taken using the preamps, the postamp/discriminators and the fastbus TDC's that will be employed for the actual E614 data acquisition. These tests were aimed at studying the efficiency and tracking precision of the drift chambers as well as the functionality of the front end electronics.

E614 has selected the VTX chip, specifications of which are listed in Table 4[11], as the preamplifier for the E614 drift and proportional chambers. It is the best choice thanks to its fast and low noise amplification, extremely low power consumption, package mass and price/ch. In addition, the VTX have demonstrated high reliability in the multi-channel spectrometers, CDF and KLOE.

Signals expected from single electron clusters will have, post VTX amplification, an amplitude of about 7-10mV and will need further amplification before discrimination. Fig. 20 shows the block diagram of the E614 amplifier and discriminator (A&D) circuit and its specifications are listed in Table 5. Fig. 21 shows, schematically the E614 frontend electronics. Prototypes, 320 preamplifier channels and 160 A&D channels, were manufactured and tested with the set of seven prototype chamber planes described above, both with particles from M13 and with sources. Two cards containing the preamplifiers were assembled to allow for tests of the chambers with the H.V. on the wires or on the cathodes, +ve and -ve polarity respectively. The frontend electronics demonstrated high stability and efficiency during these tests.

The E614 spectrometer will detect both the incoming surface muons and the positrons from the

Table 4: VTX preamplifier specifications.

Gain	1,0 mV/fc (50 Ohm load)
Dynamic range	400 mV (3% linearity at the maximum output)
Crosstalk	$\leq$ 0.3% between any two channels
Noise	860 electrons + 47e/pF (100 MHz bandwidth)
Output risetime	5 ns
Output falltime	16 ns
Input impedance	130 Ohm
Output impedance	47 Ohm
Power dissipation	10 mw/cannel (1 mA output pulldown current)
Channels/chip	6

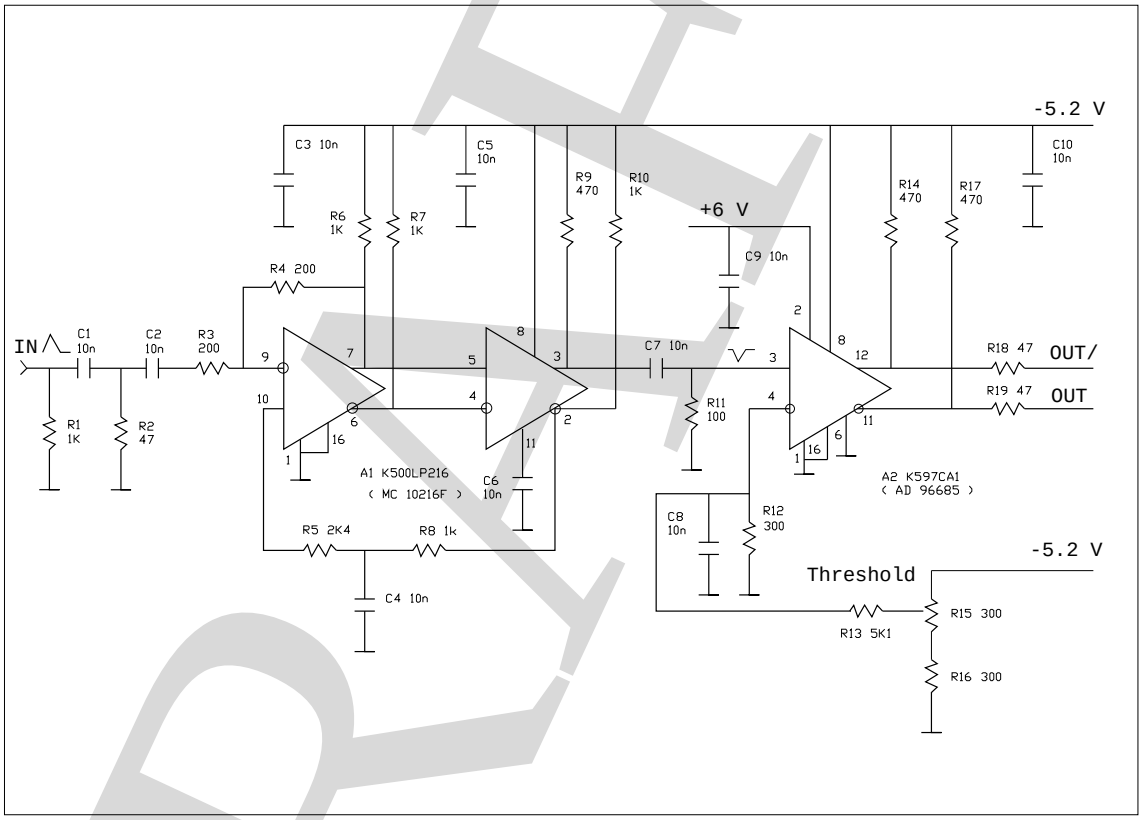

Figure 20: Schematic of the post-amplifier and discriminator.

subsequent muon decay. The energy deposited by a positron and surface muon in $4mm$ of DME gas will be $\sim$4 keV and 40-140 keV respectively. Since the system will be operated for efficient positron detection the muon signals will be large and may induce crosstalk on adjacent wires. The prototype tests have shown that a large signal from a wire does in fact induce crosstalk signals on adjacent wires.

There are two mechanisms by which crosstalk occurs. The first is that due to capacitance between the wires, between the traces on the lamel and between the channels on the amplifier boards. In this case the original signal, which has negative polarity induces a negative polarity signal on neighboring channels. To reduce this form of crosstalk, which is the most problematic since it matches the signal in polarity, the capacitances between all the components listed above. The second form of crosstalk

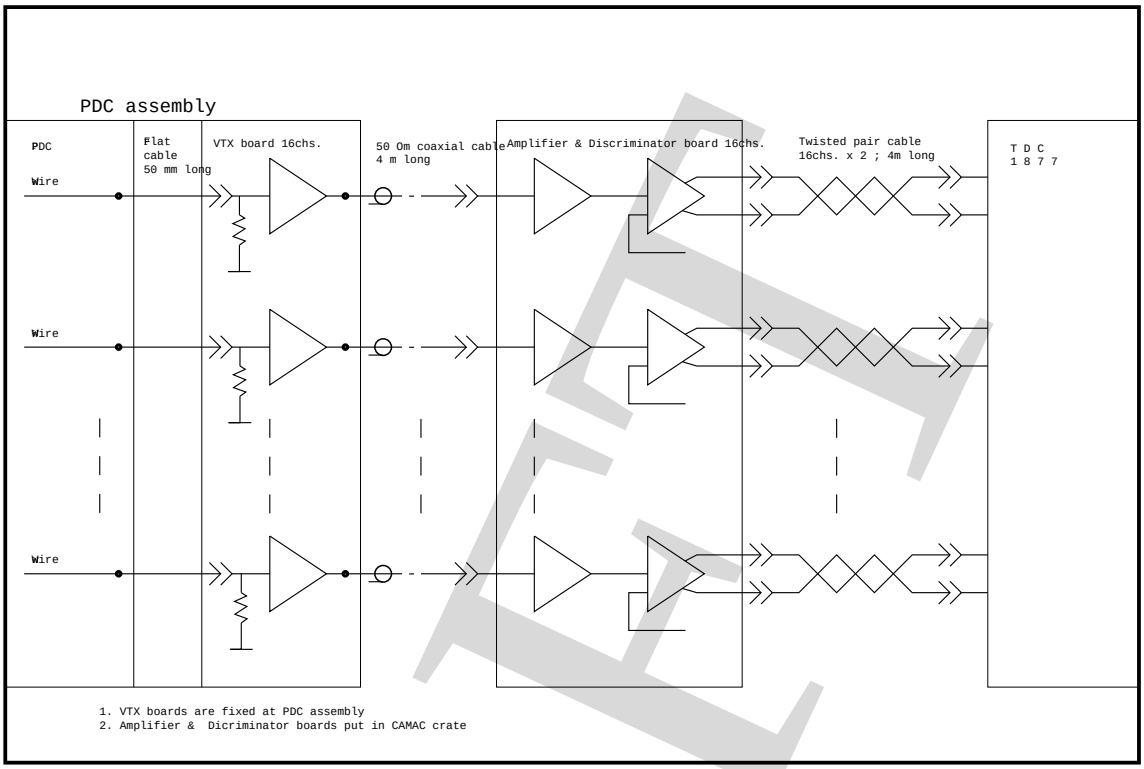

Figure 21: Schematic of the E614 front-end electronics.

Table 5: Postamplifier specifications.

Voltage gain (comparator input)	20
Output risetime	6ns
Dynamic range	400mV
Digital out	differential ECL, 110 Ohm
Number of channel	16 (32)
Package	CAMAC (VME 6U)

is due to charge conservation in the chamber. During collection of the primary ionization electrons at the sense wire a positive polarity signal is induced on the adjacent cathodes and on neighboring wires. This effect can compensate the capacitance induced crosstalk.

In order to have the cleanest possible tracking for the muon we have made calculations of the capacitance between channels on the lamel (E614 Technote 11). A lamel design that has only 0.62pF capacitance between adjacent channels was used in the full scale prototype chamber test. Figs. 22 and 23 show measurements made, at the VTX output, using an ^{55}Fe source with 1850 and 2350 volts respectively on the detector. In these figures trace 1 shows the signal on the triggered wire and trace 2 shows the crosstalk signal on the next wire. Note that the vertical scale differs by a factor of 4 between these figures. In these bench tests we have imitated the expected large muon signals with the ^{55}Fe source (5.9keV γ) by raising the H.V. appropriately. The gain of the chamber vs H.V. was determined by direct measurement of the sense wire signal amplitude to be, at 2350V, 10 times that at 1850V. This means that the signal amplitude from 55Fe at 2350V is 5.9keV x 10 = 59keV, approximately that expected from a muon at 1850V.

To detect a positron hit with very high efficiency, we found in the beam tests discussed below,

that the required threshold would be ∼14mV at the VTX output, ∼140mV at the discriminator. The crosstalk signals induced by the 5.9keV γ are $\leq$ 5 mV as shown in Fig. 22. This means that for the required 14mV threshold there will be no crosstalk induced by positron hits since the positron is expected to deposit only ∼4keV in the wire cell that was hit. The width of the crosstalk signal seen in Fig. 23 is very narrow so that the time over threshold information contained in the 1877 TDC output will serve to clean up the muon track when crosstalk is sufficient to trigger the neighboring channels.

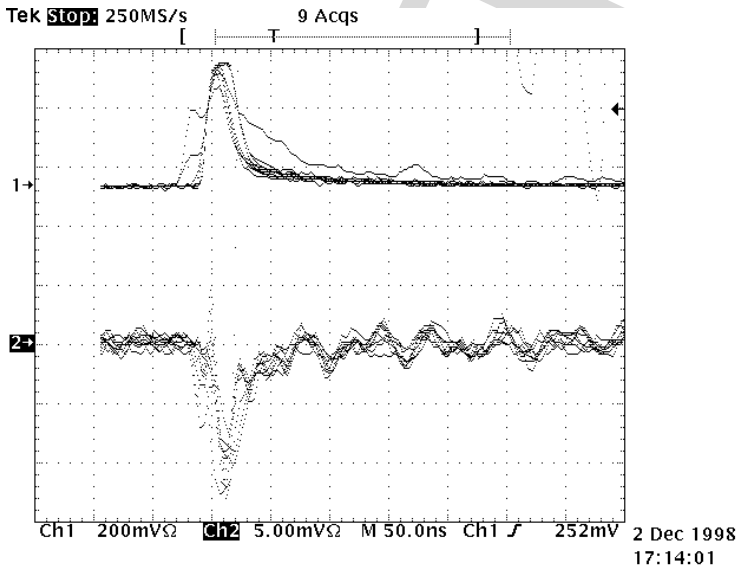

Figure 22: Signals from ^{55}Fe source with chamber at 1850 volts. Note that the channel 2 vertical scale is 5.00mV.

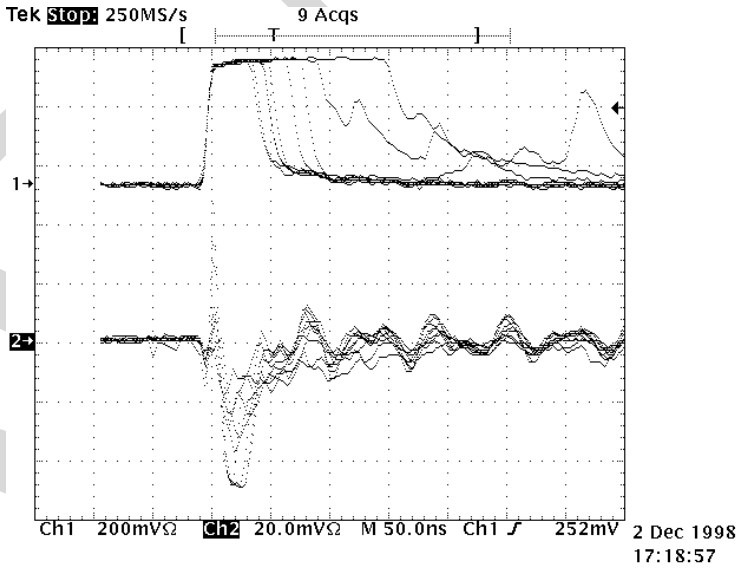

Figure 23: Signals from ^{55}Fe source with chamber at 2350 volts. Note that the channel 2 vertical scale is 20.00mV.

A typical beam test event is shown in Fig. 24, a schematic view of a pion track fitted to the drift circles in the five X planes.

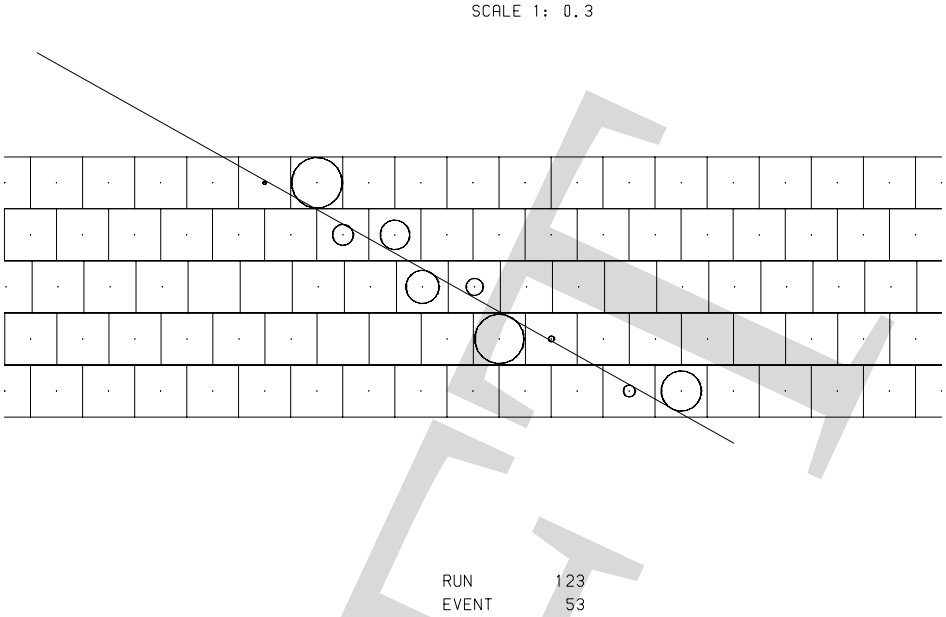

Figure 24: Schematic view of a typical pion track fitted to the drift circles in the chamber X planes.

The analysis of an event began with a search for hits that could be identified with a track. An iterative procedure was then undertaken to determine the hit position on the drift circle and the angle of the track relative to the chamber planes. Once a track was constructed, a tracking residual δd (defined as the distance of closest approach between the hit position and the track) was calculated. An average tracking residual δd_{ave} defined by

$$\delta d_{ave} = \frac{1}{N} \sum_{i=1}^{N} \delta d_i \tag{2}$$

was also calculated, where N is the total number of points used in the fit. Figure 25 shows a histogram of the tracking residuals, δd, and the average tracking residuals, δd_{ave}, obtained from the fit for data acquired at 1850 V and a chamber orientation of 0^o. The width of the tracking residuals reflects the intrinsic resolution of the chamber as well as all other factors that may contribute to inaccuracies in the tracking. This includes ingredients such as wire positions and drift distance. In addition, it reflects any biases in the fitting process, as well as the weighting used in the fit. The reasonably narrow width obtained and the level of symmetry of this histogram provides reasonable confidence in all these factors.

The tracking resolution of the chamber may be determined from the width of the tracking residuals. However, the resolution has a strong dependence on drift distance since DME is not a saturated gas. The widths of the tracking residuals were determined in 10 bins across the cell (each 200 μm wide). Since the tracking residuals themselves are dependent on the accuracy of the fit and, therefore, on the weighting of the fit (which is in turn dependent on what is assumed for the chamber resolution as a function of the drift radius), an iterative process was required. After each iteration, the widths of the 10 tracking residual histograms were determined, fitted to an eight-parameter polynomial and the results used to weight the fit. A total of 22 iterations were required for this process to converge, after which the resolutions were changing by $< 0.1 \mu m$. Figure 26 shows the result. The chamber resolution improves as a function of drift radius due to the increase in ionization statistics. This general result is independent of gas type, although DME provides high ionization compared to other gases and, therefore, both steeper improvement in the resolution as a function of drift radius and a better overall resolution. While our result is generally consistent with other experiments the min-

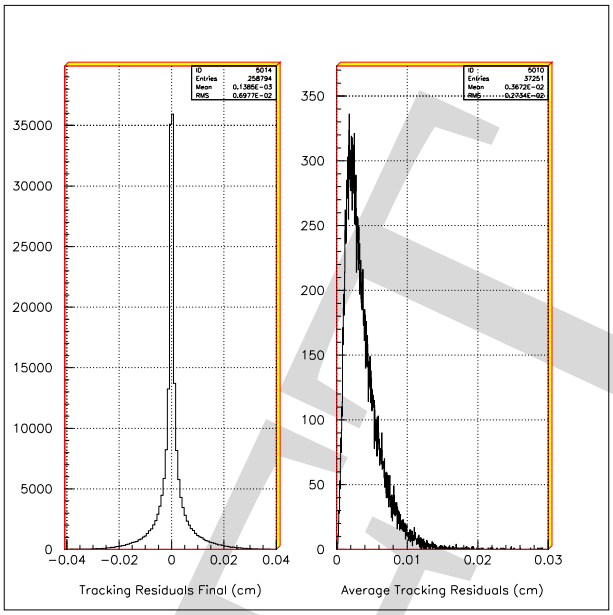

Figure 25: Tracking residuals (for each hit) and average tracking residuals (per event) for data acquired at a high voltage of $1850V$ and a chamber orientation of 0^o.

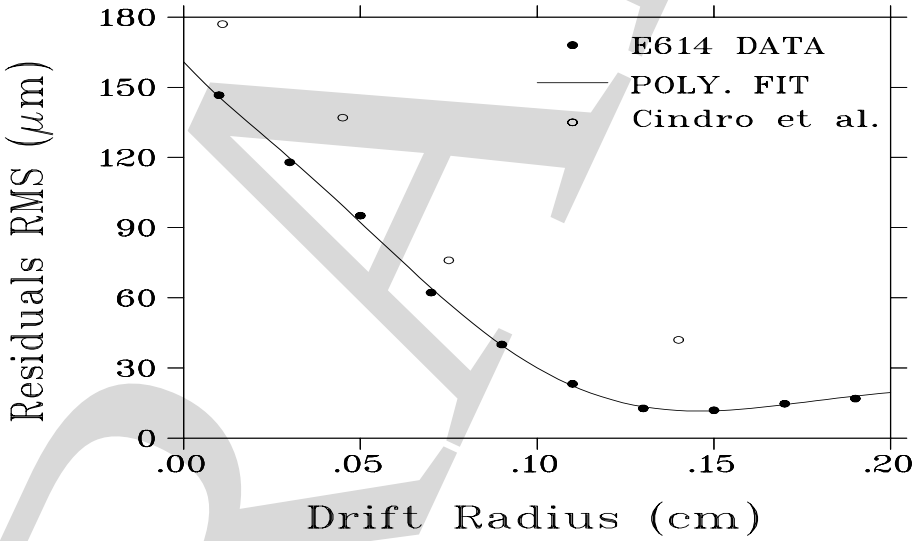

Figure 26: Chamber resolution as a function of drift radius. The dots are computed from data acquired at 1850 V and a chamber orientation of 0^0; the curve is an eight-parameter polynomial fit to the data. The circles are data from Cindro et al.[14] obtained with a drift chamber that has a cell size of $10.4mm \times 11.4mm$ and filled with pure DME gas.

imum resolution obtained (which occurs near $0.15cm$) is about $12\mu m$ in our experiment compared to $30\mu m$ for the other experiments (see for example Cindro et al.[14]). However, as mentioned above, the widths of the tracking residuals, from which these resolutions are determined, reflect the accuracy of the calibrations, tracking method etc., all of which might have contributed to the poorer resolutions obtained in these other experiments (for example inaccuracies in wire positions would smear out the total residuals).

One of the purposes of this prototype test was an important decision regarding the final chamber design, whether field wires are required between the sense wires. Installing field wires introduces disadvantages in terms of chamber construction and stability, as well as increasing multiple scattering

in the chamber. The no-field wire option is, therefore, desired based on this criteria. The lack of field wires, however, results in a weak electric field region away from the sense wires (zero at the midpoint between any two sense wires), and hits may therefore be lost due to poor electron collection from this region. This weak field region raises a concern about the chamber efficiency as a function of distance from the sense wire. To examine this effect the efficiency was calculated as a function of distance from the sense wire for 0^o runs resulting in figure 27. As expected, the lower threshold runs (140 mV) provide the best result, since signals arriving from the weak field region are expected to be small and therefore the most likely to be cut out by a high threshold. This result indicates that the chambers will have a negligible volume of slightly reduced efficiency if constructed without field wires.

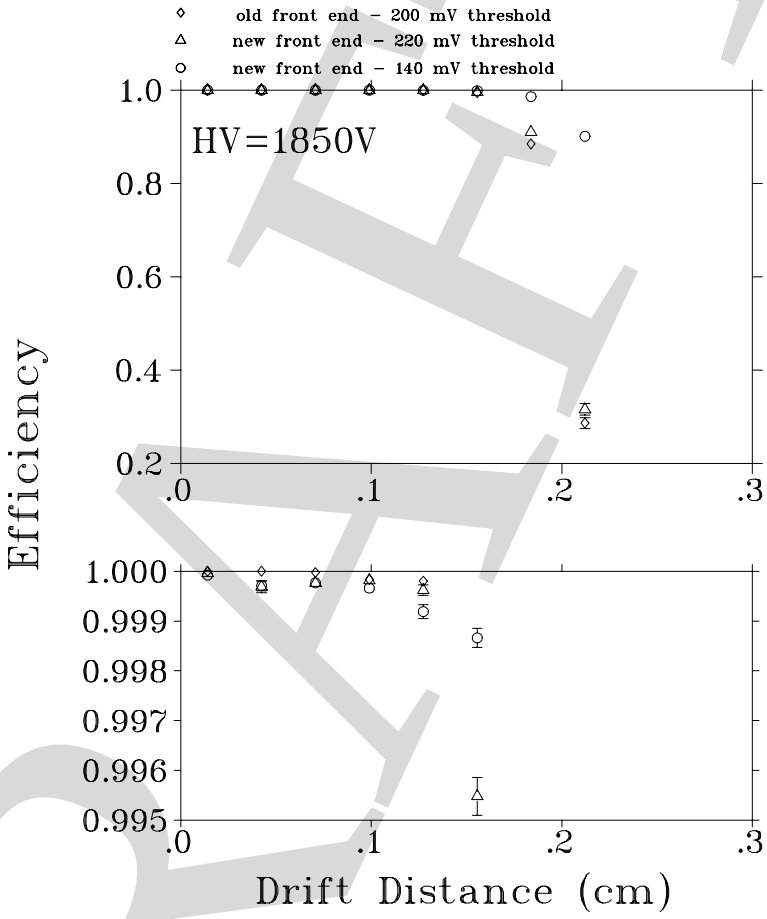

Figure 27: Chamber cell efficiency as a function of distance from the sense wire for data acquired at 1850 V with a) the old front end at a threshold of 200 mV b) the new front end at a threshold of 220 mV, and c) the new front end at a threshold of 140 mV. The bottom histogram is an enlarged copy of the top histogram.

A major conclusion reached on the basis of the above test results is that the present design, without field wires between the sense wires, will provide the efficiency and the resolution required for E614. Construction of the PDC's required for E614 has therefore begun. Another conclusion reached is that the front end electronics of the detector function as expected. Construction of the required compliment of these electronics has also begun.

The construction of the seven planes and their assembly into the prototype detector for use in this test provided much needed experience in this procedure. As a result several changes have been made in the detector design and in the assembly procedure. TRIUMF has provided a clean room specifically for the E614 detector assembly.

4 Data requirements.

An examination has been made of what requirements must be fulfilled by the data sample to achieve the high precision Michel spectrum that is the goal of the E614 collaboration. A study of the planned statistical sample of 10^9 was done to determine whether such statistics were adequate and to ascertain which angular and energy regions would provide the most sensitivity. The trigger and data acquisition issues have been studied with an eye to being able to acquire 10^9 events in a reasonable period of time. An investigation of the computing power and software needed to analyze such a large sample was made to establish what the requirements will be for these components of the E614 program.

4.1 Statistical requirements.

The E614 collaboration has developed an "analytical" Monte Carlo for those aspects of the spectrometer that could be tackled in this way. The aim was to demonstrate that the analysis of 10^9 decay events will produce significantly improved limits on the Michel parameters. In these studies the positron spectrum was generated at particular values of x and θ from the analytic equation for the Michel spectrum and binned randomly in "experimental" bins.

Since the GEANT Monte Carlo would take an extremely long time to generate 10^9 events it was decided to use the following procedure to examine the statistical requirements:

- generate positron energy spectra according to the theoretical Michel spectrum using the standard model values for the Michel parameters, at particular values of x and θ, simulating the actual binning of the experimental data;
- normalize the spectra so that the total number of events corresponds to what is expected from the experiment (i.e. 10^9);
- randomize the number of counts in each bin according to Poisson statistics (i.e. $\sigma_i = \sqrt{N_i}$);
- fit the randomized distributions, varying the Michel parameters, and determine how accurately they can be determined(the best fit parameters were found by minimizing χ^2, using a grid search technique).

The general conclusion from these studies is that statistics of 10^9 are sufficient to reach the desired accuracy for the Michel parameters(see list on page 1). Other conclusions include the fact that there is little if any benefit in attempting to measure the spectrum in the energy range below $x = 0.4$ or beyond the angular ranges $10° < \theta < 70°$ and $110° < \theta < 170°$. An unexpected but exciting conclusion is that E614 will have statistical sensitivity to the η parameter of the Michel spectrum at a level 10 times smaller than the present limit. Studies of the systematic sensitivity that E614 will have to this parameter are presently under way, the figure shown on page 1 is a rough, conservative estimate of this factor.

4.2 Data Acquisition.

The trigger will be kept as simple as possible to prevent any bias. The scintillation counter signal from the passing muon will also start a 10 μs gate to the hardware trigger module and generate a delayed STOP for the TDC's and a gate for the ADC's. If the event is rejected by the hardware trigger, it will generate a Fast Clear for TDC's and ADC's. This simple trigger will require logging most of the muon stops, hence the data acquisition system will be designed to be capable of recording 5000 ev/s. Such a requirement forces the use of readout modules with fast conversion time. Fastbus

Pipeline TDC's (1877) and ADC's (1881) from Lecroy have conversion times less than 14 μs and internal event buffering for a readout deadtime of 70 ms or 7%. The data in the internal buffers of the readout modules is read asynchronously by Fastbus Masters. This does not contribute to the deadtime as long as all the data generated by 5000 events can be read within the one second. Monte Carlo studies show that on average the muon leaves $\sim$1.5 hits/plane and the positron leaves $\sim$5 hits/plane for an average data size of 1000 bytes/ev including ADC data and software buffer overheads.

Assuming 5000 muon stops/second, the trigger deadtime would be 50ms or 5%. New Fastbus masters can read out the data from the modules at speeds $<$ 150 ns/word (4 bytes) for a readout time of 40 μs/ev. Once we include a safety factor of 2 for interrupt time, context switching , buffer setups, etc, we estimate the full readout time at $< 100\mu$s/ev. At a rate of 5000 ev/s, there would still be a factor of two before the bandwidth saturates. Data taping rates would be of the order of 10 Mbytes/s which is easily achievable with a modern workstation and 4 DLT (digital linear tape drives).

The time required for 10^9 good events under this scheme, taking into account the fact that $\sim$12% of the muons will be within the acceptable polarization cut, that $\sim$75% of these muons will stop in the stopping target and all safety factors will be of the order of one month. This time requirement will be reduced for some of the systematics studies through the use of specialized triggers. These will be generated by a trigger module using as inputs the TTL signals from the TDC backplanes. Such triggers will apply conditions on multiplicity of wires in PDC's and/or in PC's near the target to allow for, for example, rapid accumulation of wire position calibration data.

4.3 Data Analysis.

The derivation of highly precise results from $> 10^{+9}$ events will require significant computing power, hence an analysis computer will be purchased in the third year of our program. We will need to reconstruct all of the events, perhaps several times and possibly with different approaches. The results of this reconstruction will be a spectrum binned in energy and angle. To extract the Michel parameters we will compare the results to the expected spectral shape. At present, we don't know whether the "expected" shape will be derived from the theoretical spectrum, convoluted with measured and Monte Carlo response functions, or from a Monte Carlo simulation of the entire experiment. We hope to adopt the former procedure, as it will be far less computer intensive than the latter. This will be practical if the ultimate performance of the E614 spectrometer, as built, is uniform and slowly-varying in both energy and decay angle – thus, the extreme care that is being devoted to constructing the highest quality wire chambers possible. However, if we find that the actual detector non-uniformities, due for example to isolated dead wires, introduce sufficiently complex variations in the energy and angular acceptance to make a simple convolution technique unreliable, we will compare our measured spectra to a full Monte Carlo simulation of the complete data set instead.

Care is necessary in performing the final fits to avoid introducing large systematic sensitivities in the fitted Michel parameters to uncertainties in either the energy calibration or the experimental resolution. This comes about because, except in the neighborhood of $x = 1$, the Michel spectrum is smooth and featureless. Thus, the Michel parameters that one extracts from a fit bounded away from $x = 1$ are virtually insensitive to any uncertainty in the magnitudes or variations of the experimental energy and angular resolutions. The extracted Michel parameters do have some sensitivity to uncertainties in the energy calibration scale in this region, even though the spectrum is smooth. This sensitivity can usually be parameterized as a systematic uncertainty $C\Delta x$ in one or more of the Michel parameters, where C is a constant between 0.25 and 1 that depends on the specific Michel parameter in question and the form of the energy calibration error and Δx is the fractional error in the energy. By contrast, near the endpoint the steeply falling edge of the Michel spectrum implies

that the observed spectrum is characterized predominantly by its energy resolution and the precise location of $x = 1$.

Therefore, we plan to perform our fits in two stages. Initially, we will fit the endpoint region of the spectrum to determine $x = 1$ empirically and to compare our experimental energy resolution versus angle to the predictions of our Monte Carlo simulations. After we have fixed the energy calibration, we will fit the observed spectra over various energy ranges, bounded away from $x = 1$ by at least our experimental energy resolution, in order to extract the Michel parameters while minimizing our sensitivity to uncertainties in the detailed shape of the rapidly falling part of the spectrum.

5 Schedule and Budget.

Table 6 presents the Milestones that will mark the progress of E614. This schedule was extracted from the attached WBS that has been worked out in detail with the TRIUMF scheduling office. The manpower requirements of this plan will be provided by a selection of personnel from the collaborating university technical and engineering staff as well as such staff from TRIUMF. The collaboration membership will also be a source of manpower. Some of the machining of components for the spectrometer will be done at the university shops.

The magnet shield, the wire chambers, their services and their support cradle are the long term items. The aim is to have the magnet shield manufactured and the solenoid inserted and the field mapped before the first half of the wire chamber array is ready. The shielded magnet will be installed in M13 (or M11) for alignment to the beam in the summer of 2000. (E614 examined M11 in July, 1998 as a possible substitute for M13, the data is still being evaluated. At this time we continue to assume that E614 will use M13.) The first half of the detector will be inserted into the spectrometer in the late summer/fall of 2000 for alignment measurements and possibly some initial systematic studies. The entire assembly will be inserted as soon thereafter as possible, the aim being to begin full scale experimentation in the summer of 2001.

The magnet, now on site at TRIUMF, is a super-conducting solenoid that has excellent field characteristics. It is necessary to add a steel shield to this solenoid in order to contain and shape the high field and to further shape the fringe field region to minimize the transverse momentum imparted to the incoming low energy muons. For the latter purpose a separate steel collar that is referred to as a beam entry port will be manufactured to retain flexibility for alignment and shape changes. The time scale for making the required shield, the entry port and for the accurate mapping of the resulting field is about one year, thus leading to the milestone of installation in M13 for tests and alignment in the summer/fall of 2000.

The Russian group has completed the manufacture of the components for the wire chambers and the full complement of glass components are now on site at TRIUMF. Assembly of the detector has begun and it is estimated that it will require about one year to 18 months for completion of one half of the detector. Completion of the second half will require approximately an additional six months, occurring on a much faster time scale because many of the pieces will have been manufactured during the construction of the first half. The bench and beam tests of the first half of the array will take place in the spring/summer of 2000. This part of the detector will be inserted into the magnet in M13 in late 2000 where it will be employed as the upstream section of the detector for initial studies. The complete detector will be inserted into the spectrometer in the spring of 2001.

The real data will be taken at approximately 5000 events/second so that with a trigger efficiency that is estimated to be $\approx$10% it will require about one month of beam to get 10^9 good events. However Table 7 shows that a much larger amount of beam time will be required to calibrate the detector and to study the systematics influences. In total the beam time required, as is shown in this table, will be 24 months. This beam time will not all be at the full intensity available at TRIUMF,

Table 6: **Research Activity Schedule**

Milestone	Description	Start Date	End Date
Finalize Designs			
	Magnet shield	Sept. 1, 1998	June 1, 1999
	Beam entry port	Sept. 1, 1998	June 1, 1999
	Chamber support cradle	Sept. 1, 1998	Sept. 1, 1999
	Gas handling system	Jan. 1, 1999	June 1, 1999
	Cabling	Sept. 1 ,1998	June 1, 1999
	Data Aq./Slow controls	Jan. 1, 1999	Apr. 1, 2000
Manufacture			
	Magnet shield	June 1, 1999	Oct. 1, 1999
	Beam entry port	June 1, 1999	Aug. 1, 1999
	Chamber support cradle	Sept. 1, 1999	Mar. 1, 2000
	Chamber assembly & bench tests	Oct. 1, 1998	Aug. 1, 2000
	Assemble 2nd half & bench test	Mar. 1, 2000	Nov. 1, 2000
Assemble/Install			
	Assemble and map Magnet	Oct. 1, 1999	May 1, 2000
	Install Magnet in M13/M11	May 1, 2000	Aug. 1, 2000
	Install Chamber (1st half)	Aug. 1, 2000	Nov. 1, 2000
	Install Chamber (2nd half)	Mar. 1, 2001	Jun. 1, 2001
General			
Data			
	Engineering run / first data	Nov. 1, 2000	Feb. 1, 2001
	Experiment Data taking	July 1, 2001	July 1, 2004
	Publication of 1st results	$\approx$ July 1, 2003	

studies such as chamber calibrations and wire position measurements will be better served with much lower primary beam intensities. Not included in this table is the beam that will be used in the coming year for studying the beam line and for exposing the detector components to real particles as these components become available.

Using the beam time requirements from Table 7 and the beam supplied at TRIUMF in 1998 a schedule of beam usage over the life of E614 has been created. The result is shown at the top of Table 8. From this beam use schedule estimates for fieldwork travel by the E614 Canada University groups have been derived and these are shown in the lower half of Table 8. The formulae for calculating this travel requirement, shown at the bottom of this table, was derived on the basis of the present size of the E614 collaboration, 36 members, and the need to have ~ 8 people on site during beam periods. This means that the Russian and US teams will be present for beam periods according to a similar formula. The collaboration meeting contributions were calculated on the assumption of two meetings of three to four days twice a year. For the 1999-00 and 2000-01 fiscal years an additional amount of fieldwork travel has been added to cover the fact that the university groups will be coming to TRIUMF to take part in the design and construction work on the spectrometer components. As well the UofA will be sending engineering and technical personnel to TRIUMF for this purpose.

Engineering and technical people will also be provided by TRIUMF. At present an engineer has been assigned responsibility for the magnet, including its operation and testing and the finalization of the design of the shield and the manufacture of same. Several technical people have been assigned to assist with the assembly of the chambers, their front end electronics and their gas system. Designers and other technical staff will be made available as required.

Table 7: **Beam Requirements (Data & Systematics)**

Source of Correction or/and Error	Experimental Technique	Beam requirement (Months)
Coulomb scattering of muons inside the production target	Momentum change studies	3 momentum settings 3
Proton beam shift +/- 2mm	Tests and monitoring	1
Instability 10^{-3} in M13 bending magnets	Modifications, tests and monitoring	1
Fringe field depolarization	Beam tune studies and monitoring	0.5
Muon depolarization due to muon stops in last PC	Target PC ratios	0.5
Positron contamination in beam	Calibration of rejection techniques	1
Non-surface muon contamination in beam	Calibration of rejection techniques (TOF cuts)	1
Depolarization of thermal muon in metal at 2T	Study several materials.	2
Cumulative errors 2 microns in PDC's assembly	Map wire positions	n × 0.5
Random errors 20 micron in sense wire positions	Map wire positions	
Wire sag ≤1micron in PDC's	Map wire positions	
Misalignment ≤0.1mrad of B relative to beam direction	MuSR signal = misalignment ⇒ Alignment correction	0.5
PDC's misalignment ≤0.1mrad with respect to B direction	Phi dependence in spectrum ⇒ Alignment correction	1.5
Deviations: temp. 1deg. C, pressure $3^* 10^{-3}$, H.V. $3^* 10^{-3}$ in PDC's	Monitoring and controls Test/calibration data	0.5
Drift chamber zero time	PC timing ≤ 2.5 nsec. Helix fit parameter	m × 0.5
Non-uniform acceptance	Unpolarized spectrum.	4.5
Positron energy calibration	Unpolarized spectrum.	
Response function	Beam positron calibration.	0.5
Statistical errors 10^9 events	The real data	2
		19.5 + (n+m) × 0.5 ≈ 4.5
GRAND Total		24

There are presently three post doctoral Research Associates employed by E614 Canada and a forth will be spending $\sim 1/3$ of her/his time on E614. One of the full time PDF's is responsible for the assembly of the E614 planar drift chambers and proportional chambers. He has the required experience for this job and will be training and directing several other members of the collaboration in this task so that it will be completed on the time scale required. The E614 software depository and the software development will be managed from TRIUMF. A significant fraction of the development task is expected to carried out at TRIUMF. The E614 collaboration has assigned the task of development and management of the GEANT based Monte Carlo to another of the full time E614 Canada PDF's. In this task he will be coordinating the efforts of a large team drawn from the collaboration, both at TRIUMF and at the university sites in Canada and the US. He has been and will continue to be heavily involved in the employment of this Monte Carlo in studies of the spectrometer. The collaboration has named the third E614 Canada PDF as the person responsible for the development and management of the E614 analysis code. As for the Monte Carlo, this individual will be coordinating the efforts of a large team within the collaboration, including members from TRIUMF and the US and Canadian universities. He developed the initial version of this code that was employed to analyze the August 1997 prototype detector test data. The US collaborating institutes are contributing a half-time postdoc effective 1/1/99, increasing to full time by the end of 1999.

There are at present two graduate students working on the E614 project, one at the UofA and one at Texas A&M. A third, previously employed by E614 as a summer student will be joining E614 in the spring of 1999. There will be up to eight PhD theses written based on E614 data. Some of these theses will be submitted to US institutions. The number of MSc theses is potentially very large, involving the assembly, testing, mounting and calibration of the spectrometer and its components. Support has been sought for up to seven Canadian graduate students. This estimate may come to fruition soon since all the Canadian university groups are presently in the graduate student recruitment mode. E614 plans to have summer students and Co-op students employed on a continuing basis both at TRIUMF and at the UofA.

6 Systematics and tests

The complete list of corrections and errors that have been estimated for E614 (and the corresponding errors on these) are presented in Table 9 (the notation used: $(1 - P_\mu\xi)(10^{-5}) = 5 \pm 1$ means that the correction to $(1 - P_\mu\xi)$ value would be $+5 \cdot 10^{-5}$ and that the error on this correction would be $\sigma(1 - P_\mu\xi) = 1 \cdot 10^{-5}$). Several sources of these systematic errors have already been considered in other sections as noted in Table 9. Systematic error estimates for the η parameter are presently being made so they do not appear in this table.

In conclusion, we list final estimates as shown on page 1 for all of the statistical and systematic errors:

$$\sigma(\rho) = [\pm 5(stat) \pm 9.2(syst)] \cdot 10^{-5}$$
$$\sigma(P_\mu\xi) = [\pm 10(stat) \pm 10(syst)] \cdot 10^{-5}$$
$$\sigma(\delta) = [\pm 8(stat) \pm 9.5(syst)] \cdot 10^{-5}$$
$$\sigma(\eta) = [\pm 160(stat) \pm 500(syst)] \cdot 10^{-5}$$

Table 8: **Meetings, Experiments and travel plans**

	97-98	98-99	99-00	00-01	01-02	02-03	03-04	04-05
1) **Meetings**								
a) Collaboration	Aug 97	Apr 98	Jul 99	Jul 00	Jul 01	Jul 02	Jul 03	Jul 04
(2/yr)		Jan 99	Jan 00	Jan 01	Jan 02	Jan 03	Jan 04	Jan 05
2) Experiments		Months of Beam required.						
a) Chamber	M13	M11	M11	M11	M11			
tests	0.50	1.00	1.00	1.00	1.00			
b) Beam studies		M11	M11	M13	M13	M13	M13	
		1.00	1.00	0.50	1.50	2.00	2.00	
c) Experiments			M13	M13	M13	M13	M13	M13
				2.00	3.50	5.00	5.00	2.00
Total(months)	0.50	2.00	2.00	3.50	6.00	7.00	7.00	2.00

Beam studies includes low intesity running to map the wire chamberss.
Experiments assumes high intensity beam.

Team sizes: UofA 6.0 Ureg 3.0 UNBC 3.0 UMont 1.0 USask 1.0

	97-98	98-99	99-00	00-01	01-02	02-03	03-04	04-05
3) Travel to TRIUMF (man-months)								
a) UofA								
Fieldwork+++	1.50	5.00	6.40	7.80	9.60	11.20	11.20	3.20
Collaboration meetings			2.17	2.17	2.17	2.17	2.17	2.17
b) UReg								
Fieldwork	0.50	2.00	3.30	3.78	5.10	5.95	5.95	1.70
Collaboration meetings			1.14	1.14	1.14	1.14	1.14	1.14
c) UNBC								
Fieldwork	-	-	3.30	3.78	5.10	5.95	5.95	1.70
Collaboration meetings			1.14	1.14	1.14	1.14	1.14	1.14
d) Umont								
Fieldwork	-	0.50	0.47	0.82	1.40	1.63	1.63	0.47
Collaboration meetings			0.45	0.45	0.45	0.45	0.45	0.45
Total	2.00	7.50	18.35	21.05	26.09	29.62	29.62	11.95

+++ Fieldwork = No. months of beam × No. of people in group ×
.25 (each person covers 25% of beam time)

Table 9: Correction and Error Estimates.

##	Source of Correction or/and Error	$(1-P_\mu\xi)$ (10^{-5})	$(0.75-\rho)$ (10^{-5})	$(0.75-\delta)$ (10^{-5})	Disscussed in section
1	Proton beam shift ($\pm 2mm$) on the existing production target	5 ± 1	–	–	2.1
2	Coulomb scattering of muons inside the production target	5 ± 1	–	–	2.1
3	Non-surface muon contamination	12 ± 3	–	–	2.2
4	Muon decay in flight	$\ll 1$	$\ll 1$	$\ll 1$	2.2
5	The ratio $e^+/\mu^+ = 4$	$\ll 1$	–	–	2.2
6	Instability (10^{-3}) of current in M13 bending magnets	< 1	–	–	2.2
7	Muon depolarization due to muon stops in last PC	< 1	–	–	2.3
8	Creation of thin ($\ll 20$Å) films on the surface of the stopping Al target	$\ll 1$	–	–	2.3
9	Muon scattering by unpolarized electrons	1.5 ± 0.5	–	–	See Jodidio et al.[4]
10	μ Track Projection	20 ± 4	–	–	2.4.1 & 2.4.2
11	Depolarization of thermal muon in metal at $2T$	< 1	–	–	2.3
12	Deviation ($2\mu m$) of average distances in PDCs assembly	3 ± 1	5.2 ± 2	5.4 ± 2	3.2.2
13	Random errors ($20\mu m$) in sense wire positions	$\ll 1$	$\ll 1$	$\ll 1$	3.2.2
14	Wire sags ($< 1\mu m$) in PDCs	< 1	< 1	< 1	3.2.2
15	Misalignment ($< 1.0mrad$) of **B** with respect to the beam direction	< 1	–	–	3.1
16	PDCs' misalignment ($< 1.0mrad$) with respect to **B** direction	< 1	< 1	< 1	3.2.3
17	Deviation (10^{-4}) of magnetic field magnitude	± 2.5	± 2.6	± 2.7	3.1
18	Magnetic field inhomogeneity ($< 10^{-4}$)	$\ll 1$	$\ll 1$	$\ll 1$	3.1
19	Drift chamber zero time	± 5	± 5	± 5	3.2.6
20	Non-uniformity of detector acceptance	< 1	< 1	< 1	3.2.5
21	Positron energy calibration	± 3	± 5.2	± 5.4	3.2.6
22	Response function	± 5.9	± 4.6	± 4.9	3.2.1
23	Statistical errors for 10^9 events	± 10	± 5	± 8	4.1

7 Summary.

The E614 collaboration is committed to determining the Michel parameters, ρ, δ and $P_\mu\xi$ that describe the muon decay spectrum, to a precision of about $\pm 10^{-4}$ by capitalizing on a new large solid angle magnetic spectrometer equipped with a high precision array of wire chambers and using the surface muon beam from TRIUMF's M13 channel as the source of required highly polarized muons. A forth Michel spectrum parameter, η, will be determined by E614, according to present estimates, to approximately a factor of two better than present knowledge. It is possible that we will be

"scooped" on this latter measurement by a complimentary experiment at PSI involving a polarization measurement on the outgoing positron. The higher sensitivity of the positron polarization to η means that PSI would determine it to much higher precision than is possible by a specrum measurement. Such a high precisin determination would prove benificial to E614 in that it would allow us to set tighter constraints on the other parameters.

In the E614 experiment the highly polarized "surface" μ^+'s from the TRIUMF M13 beamline will enter the large volume, high field super-conducting magnet on axis and will stop in a thin target at its center. E614 has planned improvements to M13 that are designed to maintain the quality of this beam until it is delivered to the stopping target inside the spectrometer. The e^+ from the muon decay will be precisely tracked in the magnetic field using planar small cell drift chambers. This spectrometer has been simulated with GEANT and EGS4 and demonstrated to meet the precision requirements. Tests of 1/4 scale prototype chambers have been made in a magnetic field and full size prototypes of the E614 chambers have also been studied. The results indicate that these detectors will meet the E614 requirements. We will accumulate at least 10^9 events within the acceptance of the spectrometer in order to keep the statistical uncertainties to the level of the systematic uncertainties. This statistical sample can be accumulated in a very reasonable time because of the large acceptance of the spectrometer, modern electronics and modern computing power.

The construction of the E614 spectrometer has begun, the required magnet has been purchased and a data taking program will begin in the summer of 2001. The first thesis/publication from E614 data could occur as early as 2003.

References

[1] L. Michel, Proc. Phys. Soc. A63, 514 (1950).

[2] Particle Data Group. Review of Particle Physics, The European Physical Journal **C3** 1(1998).

[3] R.Openshaw, *et. al.* Nuclear Science and Nuclear Power Systems Symposium, Orlando, Nov. 9-11 1988.

[4] A.Jodidio *et.al.* Phys.Rev. D34(1986)1967-1990, ibid. D37(1988)237-238

[5] B.Balke *et.al.* Phys.Rev. D37(1988)

[6] Vector Fields Limited. (1990)

[7] B.Zhon *et.al.* Nucl.Instr. and Meth. A287(1990)439-446

[8] G.Shultz, Y.Gresser Nucl. Instr. and Meth. 151(1978) 413-431

[9] J.P. Alexander et.al. Nucl. Instr. and Meth. A283(1989)519-527.

[10] M.Kobayashi et. al. Nucl. Instr. and Meth. A312(1992)440-450.

[11] R.J.Yarema *et. al* IEEE Trans.Nucl.Sci. 39(1992)742-746.

[12] R. Fruhwirth Nucl. Instr. and Meth. A262 (1987)444-450

[13] G.Lutz Nucl.Instr. and Meth. A273(1988)349-361

[14] V. Cindro et al., Nucl. Instr. and Meth. A309(1991)411.